Combining temperature perturbations with X-ray crystallography to study dynamic macromolecules: A thorough discussion of experimental methods

Michael C. Thompson*
Department of Chemistry and Biochemistry, University of California, Merced, Merced, CA, United States
*Corresponding author. e-mail address: mthompson30@ucmerced.edu

Contents

Abstract

Temperature is an important state variable that governs the behavior of microscopic systems, yet crystallographers rarely exploit temperature changes to study the structure and dynamics of biological macromolecules. In fact, approximately 90% of crystal structures in the Protein Data Bank were determined under cryogenic conditions, because sample cryocooling makes crystals robust to X-ray radiation damage and facilitates data collection. On the other hand, cryocooling can introduce artifacts into macromolecular structures, and can suppress conformational dynamics that are

Methods in Enzymology
ISSN 0076-6879, https://doi.org/10.1016/bs.mie.2023.07.008

critical for function. Fortunately, recent advances in X-ray detector technology, X-ray sources, and computational data processing algorithms make non-cryogenic X-ray crystallography easier and more broadly applicable than ever before. Without the reliance on cryocooling, high-resolution crystallography can be combined with various temperature perturbations to gain deep insight into the conformational landscapes of macromolecules. This Chapter reviews the historical reasons for the prevalence of cryocooling in macromolecular crystallography, and discusses its potential drawbacks. Next, the Chapter summarizes technological developments and methodologies that facilitate non-cryogenic crystallography experiments. Finally, the chapter discusses the theoretical underpinnings and practical aspects of multi-temperature and temperature-jump crystallography experiments, which are powerful tools for understanding the relationship between the structure, dynamics, and function of proteins and other biological macromolecules.

1. Introduction

X-ray crystallography is a cornerstone technique in structural biology. It is responsible for a large majority of experimentally determined structures in the PDB (175,602 of 205,451 total), and has enabled the elucidation of macromolecular structures and their functional implications. While cryogenic electron microscopy (cryoEM) has stepped into the limelight recently, X-ray crystallography continues to be the workhorse for many structural biology endeavors that rely on models with high coordinate precision, derived from high-resolution experimental data. This includes drug discovery, protein design, and studies of enzyme catalysis or ligand binding. Throughout the roughly six-decade history of macromolecular crystallographic structure determination, nearly 90% of all crystal structures have been determined at cryogenic temperatures of approximately 100 K (−173 °C). The temperature at which these experiments were performed is approximately the temperature on the surface of the planet Neptune, which is quite far from the physiological conditions that are relevant to these macromolecules while they function on Earth.

Of course, there are important reasons that sample cryocooling became standard practice in macromolecular crystallography. Furthermore, despite the decidedly non-physiological temperatures used in the determination of most macromolecular crystal structures, the results of these experiments generally reflect accurate molecular details. This has been validated by decades of structural observations that were followed by judicious biochemical validation, often employing site-directed mutagenesis to test hypotheses about the relationship between structure and function.

Nevertheless, crystal cryocooling can introduce perturbations to the atomic structures of macromolecules that can obscure the interpretation of biochemical mechanisms (Fraser et al., 2011; Keedy et al., 2014; Thorne, 2023). Also, while proteins are known to be dynamic (Henzler-Wildman & Kern, 2007), a traditional limitation of crystallography has been the inherently static nature of macromolecular crystal structures, notwithstanding the information contained in atomic displacement parameters (B-factors) and sparsely modeled alternative conformations (Ringe & Petsko, 1986; Thompson, Yeates, & Rodriguez, 2020). Collecting X-ray diffraction data from macromolecular crystals at non-cryogenic and near-physiological temperatures can give a more relevant view of their atomic structures, and can provide greater insight into the conformational dynamics that underlie many important protein functions, such as enzyme catalysis and allosteric communication (Fraser et al., 2011).

Performing crystallography at non-cryogenic temperatures is now easier than ever, because modern X-ray detectors and data processing software enable diffraction measurements using low X-ray doses (Ueno et al., 2019; Winter et al., 2018, 2019). Additionally, computational tools are available that can model alternative conformations or entire conformational ensembles from experimental diffraction data (Burnley, Afonine, Adams, & Gros, 2012; Lang et al., 2010; Riley et al., 2021; Van Den Bedem, Dhanik, Latombe, & Deacon, 2009), allowing crystallographers to maximize the amount of structural and biophysical information that can be extracted from experiments at near-physiological temperatures.

With the ability to collect non-cryogenic X-ray diffraction data easily, it becomes possible to use temperature as a perturbation to map the conformational landscapes of biological macromolecules and probe their energetics. This chapter will explore the use of temperature perturbation as a tool for macromolecular X-ray crystallography, from both a fundamental and practical perspective. First, the historical reason for the prevalence of cryocooling in macromolecular crystallography will be introduced, and a brief review of the literature will demonstrate some of the hazards of sample cryocooling in macromolecular crystallography. Next, modern developments in instrumentation and software that have made non-cryogenic crystallography experiments robust and accessible will be discussed, followed by a practical description of how best to use these experimental tools. Finally, theoretical and practical aspects of using temperature as a perturbation in both static (multi-temperature) and time-resolved (temperature-jump) crystallography experiments will be discussed, including a

review of several examples that show how these experiments can be applied. This Chapter will serve as a guide for structural biologists who wish to apply these techniques in their own research.

2. Sample cryocooling in macromolecular crystallography

2.1 Cryocooling has become standard practice in macromolecular crystallography

In the late 1970s, the practice of cryocooling became standard operating procedure for the vast majority of macromolecular crystallography experiments (Haas, 2020; Pflugrath, 2015). Cryocooling involves the rapid vitrification of a crystal specimen by flash freezing in cryogenic liquid, most commonly liquid nitrogen, and maintaining the crystal at cryogenic temperature (~100 K) throughout the course of data collection. The widespread utilization of cryocooling in modern macromolecular crystallography results from a key advantage offered by the technique. Cryocooling increases the tolerance of macromolecular crystals to radiation damage, a common limiting factor for successful data collection, by approximately two orders of magnitude (Garman & Weik, 2017; Garman, 2003; Holton, 2009; Nave & Garman, 2005). Generally, the X-ray dose that is considered "safe" for a 100 μm^3 crystal at a photon energy of approximately 12 keV is approximately 0.2 MGy for crystals kept at ambient temperature during data collection, and that dose increases to approximately 20 MGy when crystals are held at 100 K. Crystals that are smaller, or contain radiation sensitive moieties, such as metal ions, are even more sensitive.

At the time cryocooling was introduced, the protective effects against radiation damage were critical for expanding the applicability of crystallography to increasingly challenging systems. For example, it enabled structural measurements for samples that yielded only small crystals, which required a large X-ray dose relative to their volume for successful data collection. Additionally, it led to more facile phasing experiments, where small anomalous differences might be sensitive to the rapid onset of radiation damage. This was especially true for multi-wavelength experiments that involved large X-ray doses and/or relatively low photon energies that exacerbate radiation damage. Importantly, it also opened the door to working with more radiation-sensitive samples, including crystals of metalloproteins and other redox-sensitive molecules that are acutely sensitive to damage resulting from photoreduction.

As synchrotron data collection became more commonplace, an additional advantage of cryocooling became critically important. As long as cryocooled crystals remain frozen, they are extremely robust to dehydration and mechanical damage, almost indefinitely. This allows for transportation of samples across the world with relative ease, and offers a straightforward solution for long-term storage. The significant advantages of cryocooling have led to its incorporation into almost every macromolecular crystallography workflow since the early 1980s

2.2 Cryocooling can cause lattice distortions that lead to practical challenges

While cryocooling provides substantial advantages described above, it also has several notable disadvantages. Practically speaking, cryocooling can be challenging. Protein crystals are, on average, about 50% solvent by volume, which leads to complications. When solvent channels and cavities in the protein crystal are large, it is possible for crystalline ice to form within these regions of the crystal (Juers & Matthews, 2004a; Moreau, Atakisi, & Thorne, 2019; Moreau, Atakisi, & Thorne, 2021; Weik et al., 2001). Even when solvent channels are relatively small, freezing of the mother liquor which bathes the crystal and keeps it hydrated during the harvesting and mounting process can form crystalline ice. When mother liquor solutions produce crystalline ice upon freezing, it is necessary to add cryoprotectants, additional solutes that promote the formation of vitreous (amorphous) ice (Pflugrath, 2015). Cryoprotection often involves high concentrations of small organic molecules, such as glycerol or ethylene glycol, salts, such as lithium chloride, or polymers, such as polyethylene glycol. The osmotic shock that results from transferring crystals from their mother liquor solution to a cryoprotectant solution can damage crystals, often leading to cracking (López-Jaramillo, Moraleda, González-Ramírez, Carazo, & García-Ruiz, 2002).

Even when cryoprotection can be effectively optimized, other physical phenomena that take place during flash cooling can damage the crystal lattice. In 2001, Juers and Matthews described a contraction of the crystal lattice upon flash cooling *Escherichia coli* β-galactosidase crystals, which was accompanied by a 50% increase in the buried surface area at crystal contacts (Juers & Matthews, 2001). Following on this observation, they performed a survey of 15 unique proteins for which both room temperature and cryogenic structures had been determined at the time, and found that on average, lattice contractions during cryocooling lead to

a roughly 4% reduction in unit cell volume. In contrast, the protein volumes are reduced by only about 1%. In 2011, Fraser et al. performed a similar analysis with 30 pairs of cryogenic and room temperature structures and found nearly identical results (Fraser et al., 2011).

The non-uniform contraction of the protein and solvent can lead to flow of solvent out of the crystal volume during the freezing process (Juers & Matthews, 2004b; Moreau et al., 2019). These effects can lead to strain within the crystal, especially when cooling rates are non-uniform (Juers & Matthews, 2004a; Kriminski, Caylor, Nonato, Finkelstein, & Thorne, 2002; Kriminski, Kazmierczak, & Thorne, 2003). All of these phenomena associated with cryocooling are potential causes of disorder that can degrade the quality of X-ray diffraction from frozen crystals, often leading to non-isomorphism (Kriminski et al., 2002) and increased mosaicity (Dobrianov, Caylor, Lemay, Finkelstein, & Thorne, 1999; Juers & Matthews, 2004b; Shaikevitch & Kam, 1981; Vahedi-Faridi, Lovelace, Bellamy, Snell, & Borgstahl, 2003). Various approaches have been developed to mitigate these complications, including hyperquenching (Warkentin & Thorne, 2007) and annealing (Kriminski et al., 2002) strategies, however, development of an effective cryocooling protocol remains a major bottleneck in the standard X-ray crystallography pipeline.

2.3 Cryocooling perturbs the structures of macromolecules

In addition to potential technical challenges, a more troubling consequence of cryocooling is that it can alter the structure and dynamics of the crystallized molecules, sometimes affecting the mechanistic interpretation of results obtained from crystallographic measurements. Following the widespread adoption of cryocooling in macromolecular crystallography, a handful of studies noted the potential introduction of artifacts into protein structures because of the procedure. For example, in 1997, Deacon et al. reported significant differences in some side chain rotamers and disordered segments when comparing room temperature and cryogenic structures of concanavalin A (Fig. 1A), and noted the number of ordered solvent molecules that could be identified in the cryogenic structure was more than double what could be identified in the room temperature structure (Deacon et al., 1997).

The potential for these cryocooling artifacts to complicate our interpretation of structure-function relationships was later highlighted by studies of two enzymes. Sandalova, et al. observed that the active site of dethiobiotin synthetase undergoes a structural transition during cryocooling

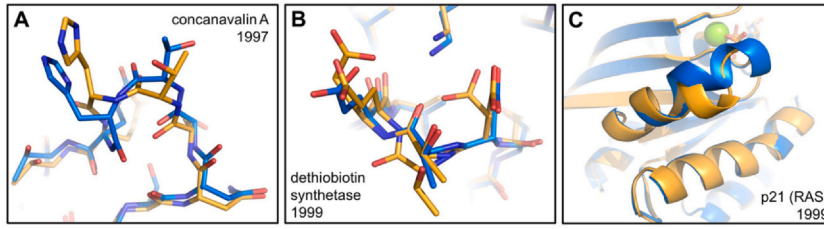

Fig. 1 Early examples of discrepancies between cryogenic and non-cryogenic protein structures. The figure summarizes findings from three papers published during the late 1990s. In each of the panels, a cryogenic structure is shown in blue, and a corresponding non-cryogenic structure is shown in orange. (A) Cryocooling results in small conformational changes in the structure of concanavalin A, including significant rearrangements of several loop regions (Deacon et al., 1997). (B) Cryocooling suppresses conformational heterogeneity and leads to other small conformational changes in dethiobiotin synthetase (Sandalova et al., 1999). (C) Cryocooling distorts the switch 2 helix in p21 (RAS) (Scheidig et al., 1999), a region that is critical for it's signaling function.

(Sandalova, Schneider, Käck, & Lindqvist, 1999) (Fig. 1B). Similarly, Scheidig, et al. noted differences in the structure of a key catalytic loop and associated active site water molecules in the switch II region of the p21(ras) GTPase (Scheidig, Burmester, & Goody, 1999) (Fig. 1C).

To address the prevalence of cryocooling artifacts, Fraser and coworkers systematically studied the distortion of side chain conformation upon cryocooling (Fraser et al., 2011). By analyzing 4008 residues across 30 proteins for which both cryogenic and room temperature structures were available, they found that 18.9% of all residues and 7.8% of buried residues change their $\chi 1$ rotamer angle significantly upon cryocooling. A growing body of work also suggests that protein–ligand interactions are potentially disrupted by crystal cryocooling (Fischer, Shoichet, & Fraser, 2015; Skaist Mehlman et al., 2023), which has important implications for drug discovery.

In addition to the structural distortions noted above, cryocooling also negates a major strength of X-ray crystallography with respect to the study of dynamic macromolecules like proteins. In a crystallographic experiment, the observed electron density is a spatiotemporal average of all conformations that are collectively explored by molecules in the irradiated crystal volume during the course of data collection. Cryocooling lowers the temperature of the sample below the solvent glass transition temperature (near 200 K) (Halle, 2004), thereby arresting protein dynamics, which are intimately coupled to the dynamics of the solvent (Fenimore et al., 2013; Frauenfelder et al., 2009).

Ideally, crystal cryocooling would be rapid enough to capture the ensemble of conformations present at ambient temperature, but in practice, cooling rates for macromolecular crystals are in the range of 0.1–1 s (Warkentin & Thorne, 2007), which is much slower than most molecular motions.

Therefore, the conformational ensemble is constantly relaxing toward a new thermal equilibrium during the flash-cooling process, with a tendency for the conformational ensemble to collapse toward compact, low-enthalpy states (Halle, 2004) that eliminate void space in the molecule (Fraser et al., 2011; Frauenfelder et al., 1987). It has already been noted that flash cooling reduces the volumes of crystallized proteins by approximately 1–1.5%. Because protein functions often involve exchange among alternative conformations, this loss of conformational heterogeneity can obscure our interpretation of molecular mechanisms from crystal structures, as demonstrated in a 2009 study of proline isomerase (cyclophilin A) by Fraser et al. (2009). In this work, the authors demonstrate that alternative conformations of the enzyme, which are critical for catalysis, were invisible in electron density maps calculated from cryogenic X-ray data but could be clearly modeled using maps derived from data collected at ambient temperature.

This study provided a powerful demonstration of the extent to which functional information can be lost during cryocooling. Additional experiments that included careful controls for X-ray dose highlighted that the increase in alternative conformations observed in non-cryogenic experiments is not due to enhanced radiation damage, and confirmed that it represents the true underlying conformational ensemble (Russi et al., 2017; Yabukarski, Doukov, Mokhtari, Du, & Herschlag, 2021).

3. Non-cryogenic macromolecular crystallography

3.1 Modern hardware and software obviate the need for cryocooling

After the introduction of cryocooling into macromolecular crystallography, experiments performed at non-cryogenic temperatures came to be viewed by most as "boutique" experiments that could be applied only to uniquely well-behaved crystal systems that yielded very large (hundreds of μm) and well-diffracting crystals, such as lysozyme, myoglobin, and RNase. This notion is rooted in the history of X-ray detector capability, and is now less true thanks to developments in both hardware and software. Given the

crystal pathologies and artifacts that can arise from cryocooling (Section 2.2), it is valuable to consider how bottlenecks to performing non-cryogenic experiments have been removed, and to understand how to utilize new technology to perform these experiments effectively.

Cryocooling is an important tool; however, one can argue that technique is overused in modern macromolecular crystallography, especially given the potential for distortion of the underlying crystal structure. There are still valid uses for sample cryocooling in a variety of experimental contexts where radiation damage is a concern (see Section 2.1). Additionally, many crystallographers have heard anecdotes or had their own experience in which only a single crystal was ever obtained for a protein of interest, yet it was enough to determine the structure. When faced with this type of scenario, it would likely be prudent to freeze your one-and-only crystal. Outside of those specific situations, most samples that can be crystallized reproducibly and are not acutely sensitive to radiation damage are suitable for non-cryogenic data collection, owing to technological developments in both hardware and software.

3.1.1 Breakthroughs in X-ray detector technology

When cryocooling was originally introduced in the late 1970s, measuring X-ray diffraction was difficult, because detector technology was still somewhat primitive. Film and image plate (Amemiya, 2008) detectors used prior to the 1990s are poorly suited for data collection at low X-ray doses needed to mitigate radiation damage, leading to the introduction of cryocooling as an enabling technology. Detectors developed throughout the 1990s, based on charge-coupled devices (CCDs) offered a variety of advantages for synchrotron data collection due to their relative speed, however they still had typically low detective quantum efficiency (DQE), typically in the range of 0.3 (Phillips et al., 1993). DQE is a measure of how much the signal-to-noise ratio is degraded by the detector electronics, with a perfect ("noiseless") detector having a DQE of 1 (Gruner, Eikenberry, & Tate, 2006). Detectors with lower DQE require more photons to be measured to achieve the desired measurement precision. Because of these detector limitations, data collection with very low X-ray dose was impossible, so sample cryocooling was revolutionary. In the ensuing decades cryocooling became a standard practice that enabled many new experiments and an explosion of structural data.

The mid-2000s ushered in a technological breakthrough in commercial X-ray detector technology that makes non-cryogenic data collection

routine. Specifically, during this period, the pixel-array detector (PAD) became part of the standard instrumentation available at many macromolecular crystallography beamlines across the world. These devices have several advantages over their predecessors, namely CCDs, in terms of their speed and detection properties. Critical to their utility in non-cryogenic experiments is the fact that PADs are direct photon counting detectors, which can have single-photon sensitivity and DQE values approaching 1 (Förster, Brandstetter, & Schulze-Briese, 2019). This allows for measurements with high signal-to-noise, even at very low X-ray doses. With the ability to measure weak but reliable diffraction using doses as low as tens of kGy, radiation sensitivity is a lesser problem for many macromolecular crystal systems, even when crystals are small or otherwise sensitive. The weak signal resulting from low dose per image can be overcome with high data multiplicity and merging of the integrated reflection intensities.

3.1.2 Integration of weak reflection intensities with modern software

The ability to reliably measure X-ray diffraction patterns with single-photon sensitivity required data processing algorithms that could operate with very small signals. Specifically, crystallographic data reduction software needs to reliably find reflections that can be used for indexing, and then to integrate them accurately (with background subtraction) prior to merging. When working with very low X-ray doses, data reduction programs that fit pixel intensities against an empirical reflection profile, such as DIALS (Winter et al., 2018) and XDS (Kabsch, 2010), are known to give better estimates of weak reflection intensities (Diamond, 1969). One might recommend that one of these data processing programs be used for indexing and integration of weak data resulting from low X-ray doses. In 2012, a groundbreaking paper by Karplus and Diederichs (Karplus & Diederichs, 2012) demonstrated that useful signal can be extracted from much weaker (lower $I/\sigma(I)$) diffraction data than was previously appreciated (and introduced the useful statistic CC1/2). This revelation further validated the use of low X-ray doses in macromolecular crystallography, especially for non-cryogenic measurements.

3.2 Practical considerations for non-cryogenic data collection

When performing non-cryogenic crystallography experiments, there are two major challenges that the experimenter must be aware of and work to mitigate—avoiding crystal dehydration and not exceeding the relatively low X-ray dose threshold for radiation damage. These two key

considerations, relevant at the sample preparation and data collection stages of the experiment, respectively, are critical for success and also require procedures that are markedly different from what one would do during a cryocrystallography experiment.

3.2.1 Sample preparation

The first branch point where the non-cryogenic macromolecular crystallography workflow deviates from the common procedure for working with frozen crystals is at the stage of crystal harvesting and mounting. This stage of sample preparation is critical for protecting the crystal from dehydration during data collection, which is more challenging when crystals and their surrounding mother liquor are not frozen, which we noted above as a major advantage of cryocooling. An additional benefit of cryocooling, which has not been mentioned yet, was the introduction of the cryoloop (Fig. 2A), a small polymer lasso that can be used to capture a crystal from its growth solution with little excess solvent, and then to plunge it directly into a cryogen such as liquid nitrogen (Pflugrath, 2015).

Before introduction of the cryoloop, the traditional method of preparing macromolecular crystals for X-ray diffraction experiments involved the assembly of complicated "capillary mounts" (First Analysis of Macromolecular Crystals | Springer Nature Experiments, n.d.) (Fig. 2B). In this procedure, an experimenter carefully manipulates a crystal into a thin-walled glass capillary tube using a pipette or syringe, and then uses a small wicking device (a tiny sliver of filter paper) to remove just the right amount of excess mother liquor from the crystal to keep the specimen hydrated without producing excessive background scattering. A small volume of excess mother liquor is left inside the tube, and the ends are sealed with wax or glue before affixing to a goniometer base for data collection. Mounting protein crystals, which are delicate and sensitive to humidity, is far easier to do with a cryoloop than with a capillary mount. Current best practices for preparing samples for non-cryogenic X-ray diffraction experiments combine the simplicity of cryoloop mounting with various physical or chemical barriers that protect the crystal from dehydration, rather than with plunge freezing.

The most common approach to preparing crystals for non-cryogenic data collection is essentially a hybrid of the cryoloop and capillary methods (Fig. 2C). This approach is straightforward, and the required materials are available commercially. Specifically, the method requires a standard cryoloop with a magnetic goniometer base and a 2 mm internal

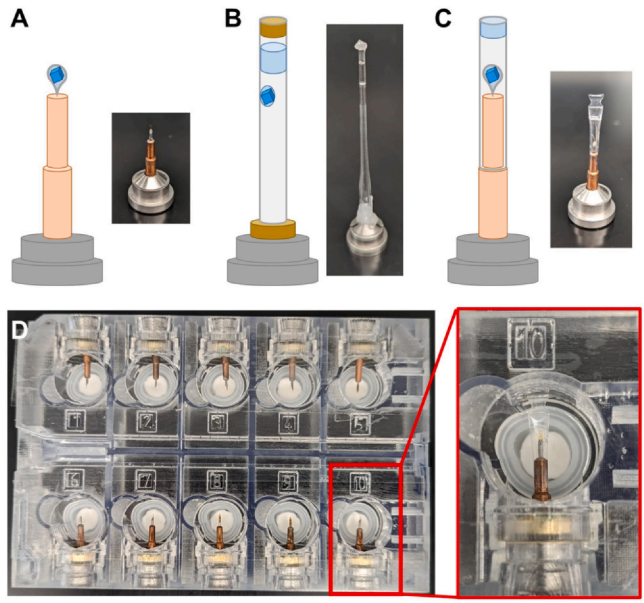

Fig. 2 Crystal handling for non-cryogenic experiments. Different crystal mounting methods are shown as cartoon alongside a photo of a prepared mount. (A) The cryoloop, used commonly for cryogenic crystallography experiments consists of a polymer loop at the end of a metal pin that is affixed to a magnetic goniometer base. The loop can be used to isolate a crystal and then plunged into cryogen to freeze the crystal. Ideally, the size of the crystal (bright blue) is well-matched to the size of the loop as shown to reduce background scattering. (B) The original method for preparing macromolecular crystals for non-cryogenic data collected is known as a "capillary mount." A thin glass capillary contains a hydrated crystal stuck to the inside surface of the capillary, as well as a small volume of crystal mother liquor to keep the crystal hydrated (light blue). The capillary is sealed at both ends with wax (yellow), and affixed to a goniometer base. The preparation of capillary mounts is laborious compared to freezing crystals in cryoloops. (C) A hybrid system allows crystals to be prepared for non-cryogenic data collection by harvesting them in a cryoloop, and then sealing the cryoloop with a thin polycarbonate capillary that is closed at one end. The plastic capillary also contains a small volume of crystal mother liquor to keep the sample hydrated, like a capillary mount. (D) A commercial plate system is available for shipping crystals prepared for non-cryogenic data collection. Each well contains a disposable fiber plug that can be soaked with crystal mother liquor to maintain a humid environment. Crystals are inserted into the wells of the plate through a hole in the side that grips the magnetic base of the cryoloop. The top of the well is sealed with a water impermeable tape.

diameter, thin-walled polyester capillary, which is sealed on one end. Such cryoloops have become ubiquitous in macromolecular crystallography, and the tubing is available commercially. The procedure begins

by cutting the capillary at the open end to roughly match its length to that of the cryoloop, and then pipetting a small amount (~4 μL) of crystal mother liquor into the sealed end of the capillary. Next, a crystal is harvested from its growth environment using a standard cryoloop with a magnetic goniometer base. The process of harvesting the crystal from its growth environment mirrors the way in which crystals are typically harvested for cryocooling. However, rather than plunging the harvested crystal into cryogen, the loop is placed upright, and the polyester capillary is drawn down over the sample and sealed to the goniometer base using a small amount of vacuum grease. The assembly retains the advantages of a traditional capillary mount—the water-impermeable polyester capillary and vacuum grease create a dehydration barrier, while the small plug of mother liquor maintains an appropriately humid environment to keep the crystal hydrated—but does not require challenging crystal manipulations that can damage the specimen. The thin polyester tube produces a relatively low amount of background scattering, which is beneficial for data quality.

Another useful method for preparing crystals for non-cryogenic data collection involves the combination of a cryoloop with chemical barriers to dehydration, usually some type of highly viscous and water impermeable oil. Commonly used oils are proprietary mixtures (chemical compositions unavailable) known as "NVH Oil" and "Parabar" (or "Paratone"), which are available commercially. The idea is simple in principle—the crystal is mounted in a cryoloop and coated in oil to prevent dehydration. This method can be highly effective, but the procedure can be challenging and requires practice for most experimenters. Once again, a crystal is harvested from its growth environment using a standard cryoloop with a magnetic goniometer base, and it is transferred into a small droplet of oil. The crystal must be fully immersed in the oil, and carefully manipulated to strip away excess aqueous mother liquor from around the crystal. Once this has been done successfully, the cryoloop can be used to remove the oil-coated crystal for data collection.

Although the process seems straightforward, there are several significant challenges. First, the oil is very viscous, and maintaining a coating around the crystal at non-cryogenic temperatures while manipulating the crystal in the oil can result in mechanical damage if not done carefully. Next, the refractive indices of the useful oils are generally very close to the refractive indices of protein crystals, which means that most crystals become invisible when they are well-coated in oil. Using a microscope

with a cross-polarizer can help overcome this challenge. Finally, this method is quite unforgiving, and it is essential to make sure that the mounted crystal is completely covered in oil, otherwise it will not be sufficiently protected from dehydration. For this reason, some crystal morphologies are not ideal for this method, especially those with sharp vertices and edges that tend to poke out of the oil and create an "Achilles heel" for crystal dehydration. Although it can be difficult to execute, the high-viscosity oil method works extremely well if executed properly, because the oil creates a barrier that is completely impermeable to water vapor. This maintains the crystal under the same hydration conditions it was grown in, unlike the capillary method, in which vapor diffusion can occur within the capillary. Adaptations of this method include sealing the cryoloop-mounted crystal with more exotic materials, including polymer glues (Baba, Hoshino, Ito, & Kumasaka, 2013) and graphene (Warren et al., 2015), but these procedures require specialized materials and/or equipment.

Regardless of the sample mounting method (capillaries or oils), there are three important and general considerations for preparing samples for non-cryogenic data collection. First, when preparing crystals for non-cryogenic data collection, it is obviously not necessary to add cryoprotectants to prevent the formation of ice. However, if the goal of an experiment is to compare structures at cryogenic versus non-cryogenic temperatures (see Section 4), it can be useful to add any cryoprotectants that were utilized for the cryogenic data collection. Cryoprotection often involves large changes to the solution conditions (López-Jaramillo et al., 2002), and treating crystals in an identical manner prior to data collection at different temperatures can circumvent uncertainty about whether any observed structural differences are due to temperature or differing solution conditions.

Second, it is important to select an appropriately-sized cryoloop for the crystal specimen. This is not really necessary in cryocrystallography, because after the crystal is mounted and frozen, it is virtually immobile on the loop; it can be larger or smaller than the loop. In a non-cryogenic experiment, mother liquors and oils that surround the crystal remain liquid, and therefore if the crystal is small relative to the volume of liquid in the loop, it can move within the loop as it rotates during data collection, resulting in data that are difficult to interpret. On the other hand, crystals become more prone to drying out in capillaries or poking out of oil coatings if the loop is too small relative to the size of the crystal.

Third, non-cryogenic crystallography experiments often involve transportation of crystal trays to the X-ray facility, or crystal growth on-site, followed by mounting of the samples immediately before data collection. This can be logistically difficult for researchers that are not close to an X-ray facility. It would reduce throughput if samples must be prepared during the experiment, rather than in advance. Recently, shippable humidity chambers were developed and commercialized that enable the transportation of mounted crystals at ambient temperatures (Fig. 2D). These chambers can be pre-loaded with samples (prepared using either capillary or oil methods) and shipped or transported in a thermally-insulated container to the experimental facility for data collection. The development of these tools will likely be transformative for the widespread adoption of non-cryogenic crystallography because it lowers a major barrier. This will be especially true if these tools for non-cryogenic experiments are integrated into remote data collection programs at synchrotron facilities.

3.2.2 Data collection

In a reference to the Wild West, the pioneering protein crystallographer Michael Rossmann often joked about the "American Method" of crystallography, in which one could "shoot first, and ask questions later" (Wu & Arnold, 2019). Initially, this phrase referred to the benefits of autoindexing algorithms [developed by Rossmann himself (Steller, Bolotovsky, & Rossmann, 1997)] that could identify the unit cell regardless of crystal orientation relative to the beam. The haphazard approach to data collection was only reinforced by cryocooling procedures that made samples robust to large X-ray doses that yielded visibly strong diffraction patterns.

Removing some of the barriers to successful data collection enabled high-throughput experiments, and made crystallography accessible to the non-expert, both of which were critical for the development of structural biology as a field. Indeed, in 2023 most data sets are collected in this manner, with a relatively high X-ray dose (20–30 MGy) being distributed over a large (e.g. 360°) wedge of reciprocal space, ensuring satisfactory completeness of the data regardless of the space group. Despite the advantages of the "American Method," collecting data at non-cryogenic temperatures requires a more thoughtful approach so as not to exceed the relatively low X-ray dose threshold for radiation damage under non-cryogenic conditions.

The approximate dose threshold for radiation damage under non-cryogenic conditions, which is approximately 0.2 MGy for a 100 μm^3 crystal at a photon energy of approximately 12 keV (Garman & Weik, 2017), has

already been discussed (Section 2.1). For crystals that are larger or smaller than 100 μm^3, it will be necessary to adjust the dose. A variety of tools are available for determining the appropriate X-ray dose for non-cryogenic data collection, the most comprehensive of which is RADDOSE-3D (Bury, Brooks-Bartlett, Walsh, & Garman, 2018). These tools take various crystal, X-ray beam, and experiment parameters as input, and calculate the required X-ray dose and ideal data collection strategy for non-cryogenic experiments. This total X-ray dose can be converted to a dose rate in terms of Gy/s or photons/s for a given size X-ray beam, so that the source parameters can be adjusted appropriately. Please note that the X-ray dose used for non-cryogenic data collection is approximately two orders of magnitude less than what is used for cryogenic experiments (Garman & Weik, 2017). This can make the diffraction images appear very sparse, and sometimes nearly blank, but the detector will be able to measure reflections that are too weak be visualized on the computer screen (Fig. 3).

To get a sense for how well crystals actually diffract, it is often useful to sacrifice a sample and collect a single image with 10–20 times the planned dose, so that high-resolution diffraction is clearly visible. This will provide

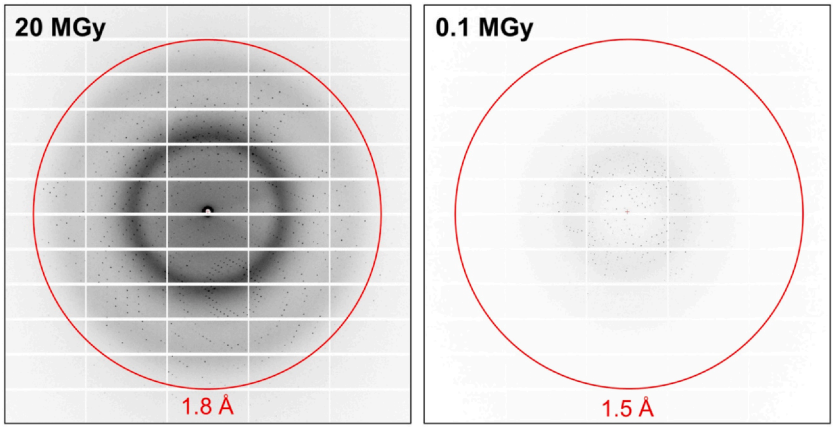

Fig. 3 X-ray diffraction under high and low dose regimes. X-ray diffraction images are shown that are collected from identical protein crystals, using a different X-ray dose. The images are displayed on the same intensity scale. The image on the left was collected with a high (20 MGy) dose, and the overall signal appears as most crystallographers would expect from a crystal that diffracts well. The image on the right was collected with 200-fold less dose than the image on the left (0.1 MGy), and only the very strongest reflections are visible at low resolution. Nevertheless, the data set corresponding to the image on the right can be integrated and merged to a resolution of 1.7 Å using only 180 images collected using this low dose.

feedback on crystal quality and will help position the detector at the correct distance from the sample. Note that the higher dose per image does not make the crystals diffract better, it simply makes the reflections more visible to the human eye on a computer screen. With a highly sensitive PAD, the weak reflections can be accurately integrated (Ueno et al., 2019; Winter et al., 2019). As described in Section 3.1.2, the weak individual images may lead to a lower-than-expected overall ratio of $I/\sigma(I)$ for the integrated and merged data, however the correlations between unique reflection measurements (as measured by $CC_{1/2}$, for example) should remain strong. Certain data reduction programs (Kabsch, 2010; Winter et al., 2018) are better-suited to handle these weak reflections (Diamond, 1969).

After determining the desired X-ray dose for a particular crystal, one must consider how the dose will be distributed evenly throughout the crystal volume. The simplest strategy for doing this is to closely match the beam size and the crystal size, so the entire crystal volume remains bathed in the beam throughout the entire rotation series (Fig. 4A). Most X-ray beams are focused and subsequently shaped with apertures so that their cross-section is roughly circular. Many beams have adjustable sizes via the insertion of different apertures or via adjustable focusing (Evans, Axford, & Owen, 2011; Fuchs et al., 2014). Beams that can be adjusted via focusing are advantageous because their size is the most variable, but due to the behavior of synchrotron radiation these beams are often non-circular, with dimensions that are broader in the horizontal direction than in the vertical, leading to non-circular shapes. When possible, instrument adjustments should be used to closely match the crystal size and beam size, so the dose is inherently distributed across the entire crystal.

Distributing the X-ray dose evenly across the crystal volume is the most straightforward when the crystal is roughly the same size in all three dimensions; this is rarely the case. Crystals that are substantially longer in one or two dimensions require translation of the sample to distribute the dose throughout the crystal volume, and can also require other compromises. In order to facilitate crystal translation during data collection, it is desirable to mount the crystals so that their longest physical dimension is roughly (but not necessarily exactly) parallel to the goniometer rotation axis (Fig. 4B,C). Because most diffractometers allow crystal translation along the goniometer rotation axis, samples that are mounted in this way can be effectively moved through the X-ray beam during data collection, to distribute the dose throughout the largest possible crystal volume.

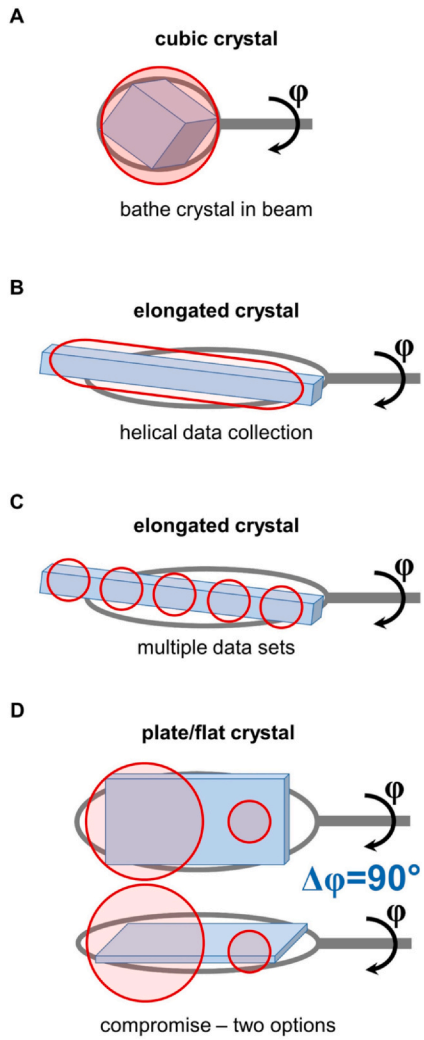

Fig. 4 Strategies for low-dose X-ray data collection. A key aspect of mitigating radiation damage during X-ray data collection, especially for non-cryogenic samples, is to distribute the X-ray dose throughout the crystal. The cartoons depict differently shaped crystals held in cryoloops that are rotatable about a goniometer φ axis. In each case, the footprint of the X-ray beam during data collection is outlined in red, and shaded according to the approximate dose deposited over the underlying area. (A) If the crystal is roughly the same size in all dimensions (cubic) then one can simply match the size of the X-ray beam to that of the crystal. Elongated, rod-shaped crystals can be treated in one of two ways. (B) Helical data collection can be implemented, in which the crystal is translated during the measurements, so that the entire crystal volume is measured probed during the collection of a single data set. (C) Another strategy for collecting data from elongated crystals is to collect a full data set from each of several locations on the crystal, using a lower overall dose for each individual data set. (D) When crystals are small in a single dimension only (flat/plate crystals), then one must make a compromise on whether to match the beam to the larger or smaller dimension of the crystal about the rotation axis.

There are two distinct approaches to data collection from an elongated crystal via sample translation, and both will be considered in light of the following example. Consider a crystal that is 1000 μm × 100 μm × 100 μm (a rod shape), mounted roughly parallel to the goniometer rotation axis, a desired data collection wedge that includes 180° of reciprocal space with 1° oscillation per image and a total dose of 180 kGy. Assume an X-ray beam with a diameter of 100 μm, and hard edges (n.b. most X-ray beams do not have perfect edges, but this simplification makes the following considerations simpler).

The first, and most common, strategy for doing this is referred to as "helical" data collection (Polsinelli et al., 2017; Rajashankar & Dauter, 2014). In this approach, the crystal is translated simultaneously in all three directions as it is rotated during data collection, so that fresh crystal volume is continuously brought into the beam, and expended crystal volume is removed from the beam (Fig. 4B). Many synchrotron beamlines have implemented helical data collection into their control software. Assuming the above example, a helical data collection strategy will yield 180 images, each covering 1° of reciprocal space. If the total dose is 180 kGy, then the dose per image is 1 kGy. If we translate along the length of this crystal, a particular region will be exposed for 18 consecutive images, and receive a dose of 18 kGy. When the data are collected in this way, each region of the crystal is sampled across 18° of reciprocal space.

The second, and less commonly implemented strategy, involves collecting non-overlapping and individually complete data sets across the length of the crystal, each utilizing only a fraction of the total desired dose (Fig. 4C). Assuming the above example, this data collection strategy will yield 10 unique, non-overlapping data sets, each containing 180 images and collected with 18 kGy total dose. Each of the 10 data sets can be integrated individually, and then merged appropriately. In this case, the dose per image is only 0.1 kGy. The composite data set will contain 1800 images, and 180° of reciprocal space have been sampled at each position on the crystal.

Given the two strategies outlined above, the one which is most appropriate to use for a particular experiment depends on several factors. First, if the diffractometer control software is not capable of helical data collection, then there is no choice but to implement the second strategy, where multiple unique data sets are collected. Next, the type of detector becomes a consideration. The differences between older CCD detectors and newer PAD devices have already been mentioned (Section 3.1.1), and the important difference between the two is the DQE, which is much higher for PADs than for CCDs, which makes them much more sensitive.

A consequence of this is that PADs are much more effective at measuring weak diffraction signals. If a CCD is available, it might be desirable to have a high per-image X-ray dose of 1 kGy that results from the helical strategy, rather than the low per-image X-ray dose of 0.1 kGy that results from the multiple data set approach. On the other hand, if a PAD is available, then it should be possible to detect the diffraction signal in the weaker, low dose images, and effectively merge the integrated reflections.

Finally, crystal quality is an important consideration. In the case of a perfect crystal, there should be no difference between the two strategies; however, crystals are never perfect. One can demonstrate that even within a single macromolecular crystal, there can be domains that are non-isomorphous with one another (Gallagher-Jones et al., 2020; Thompson, Cascio, & Yeates, 2018). The helical data collection strategy results in different regions of reciprocal of reciprocal space being sampled from different regions of the crystal. Therefore, if a particular region of the crystal is not isomorphous with the rest, the composite dataset can be rendered useless due to incompleteness. When using the multiple data set approach, complete data sets are collected for each region of the crystal, and if one or more regions are non-isomorphous, they can simply be excluded from the final, composite data set. Unit cell clustering algorithms are available to aid in this process (Foadi et al., 2013; Gildea et al., 2022; Soares et al., 2022; Thompson et al., 2018; Zeldin et al., 2015).

In the case of plate-like crystal morphologies, in which the crystals are large in two dimensions, but small in the third, a compromise must be made (Fig. 4D). The crystal can still be translated along its longest dimension, but a choice must be made with respect to the beam size. On one hand, data can be collected with a beam that matches the second largest dimension of the crystal. In this case, the same volume of crystal remains in the beam during rotation, but there will be more background air scatter due to the larger beam. On the other hand, the beam can be made to match more closely to the smallest crystal dimension. This reduces the background scattering, but the diffraction will be stronger for some crystal orientations than for others, because different crystal volumes will be exposed to the beam as a function of rotation angle.

3.2.3 Multi-crystal approaches and serial crystallography

Section 3.2.2 above described a data collection strategy in which 10 essentially unique data sets were collected from a single crystal and merged, based on their isomorphism. This same strategy can be applied to data

collection from 10 (or more) different crystals. By collecting multiple data sets from many different crystals, it becomes possible to collect high-multiplicity data with essentially infinitely high X-ray doses, because the dose can be spread over any number of individual samples. The individual data sets are indexed and integrated as independent single-crystal data sets, and then merged to improve signal-to-noise.

Well-established data reduction programs, such as XDS (Kabsch, 2010) or POINTLESS/AIMLESS/TRUNCATE (Evans, 2006), have options to merge multiple data sets. Once again, before merging, algorithms that cluster data sets based on unit cell isomorphism are important for determining which data sets can be combined (Foadi et al., 2013; Thompson et al., 2018). In a multi-crystal experiment, full data sets (i.e. 180° of reciprocal space) or partial data sets can be collected from each individual crystal. If partial data sets are collected, it is important that the multiple crystals measured are in different orientations, so that the merged data set is complete.

An advantage to collecting partial data sets is that the individual images can be measured using a higher X-ray dose, because only a fraction of reciprocal space needs to be sampled before a given crystal succumbs to radiation damage. To facilitate multi-crystal experiments, a variety of different mounting supports have been developed that allow the preparation of multiple crystals on a single device, to minimize the need for sample changes. These include a variety of polymer grids (Baxter et al., 2016), meshes (Nam, Kim, & Cho, 2021; Park, Choi, Eo, Cho, & Nam, 2020), and chips (Gilbile et al., 2021; Lyubimov et al., 2015; Murray et al., 2015; Perry et al., 2014; Saha et al., 2023; Sui et al., 2021) that can be affixed to a standard magnetic goniometer base. Additionally, plate goniometers are available that allow data collection from crystals directly in the crystallization plate, allowing the *in situ* measurement of multiple crystals without removing them from their growth environment (Hargreaves, 2012; Okumura et al., 2022). Because it is impossible to cryocool an entire crystallization plate efficiently, these in-situ measurements are always performed at ambient temperature. Solid sample supports and plate goniometers are generally limited in the accessible rotation angles during data collection, so these strategies rely on the random orientation of different crystals on the support or in the tray.

The most extreme case of multi-crystal X-ray crystallography experiments are those which are referred to as "serial crystallography" (Gruner & Lattman, 2015; Mehrabi et al., 2021; Schlichting, 2015). In these experiments, rather than using relatively large, single crystals that are tens to

hundreds of μm in each dimension, researchers prepare slurries of microcrystals, that are on the order of 1–20 μm in all dimensions. In contrast to rotation crystallography, where a single crystal rotated in the X-ray beam to obtain a complete (or partial) data set, in the serial crystallography experiment, each crystal produces just a single diffraction image representing a random slice through reciprocal space. One reconstructs a complete diffraction pattern by measuring, processing, and scaling together thousands of randomly oriented crystals (Boutet et al., 2012; Chapman et al., 2011), producing a random sampling of reciprocal space. This approach allows a large X-ray dose to be used for each image, effectively destroying the crystal in a single shot.

When performed at a synchrotron (Martin-Garcia et al., 2017; Owen et al., 2017; Schulz, Yorke, Pearson, & Mehrabi, 2022; Weinert et al., 2017), one measures individual diffraction images with tens of kGy, typically delivered in milliseconds or less. This constitutes a relatively low dose for the crystal, but a high dose for an individual image (De La Mora et al., 2020). When the experiment is performed at an X-ray free electron laser (XFEL) (Boutet et al., 2012; Chapman et al., 2011), the data are collected using ultrafast X-ray pulses that are roughly 30 fs in duration, but deliver approximately 10^{12} photons per pulse. The peak power of these pulses is so high that they cause the crystals to undergo coulombic explosion, however they are also so fast that the diffraction patterns are collected before the onset of any damage. This approach, which has been referred to as "diffraction before destruction," provides structural data that is ostensibly free of the effects of radiation damage, even at non-cryogenic temperatures, provided that the X-ray pulses used in the experiment remain short (<50 fs). The nature of these experiments, in which each crystal specimen contributes a single diffraction image to the data set prior to its destruction, requires that the sample be continually refreshed in the X-ray beam. This requirement is the defining feature of the technique that inspired the name "serial" crystallography.

From a practical standpoint, serial crystallography experiments differ from standard rotation experiments in two main ways, alluded to above. The first has to do with sample preparation and delivery of crystals into the X-ray beam. As noted, serial crystallography requires a slurry of microcrystals suspended in mother liquor. In favorable cases, tens to hundreds of microliters of crystal slurry are sufficient to determine a crystal structure in a serial experiment (Weierstall et al., 2014), however some experiments can consume milliliters of this slurry. Therefore, it is necessary to have a reliable

method for growing large volumes of microcrystals, preferably in a batch format. A straightforward and reliable protocol for adapting traditional crystallization conditions, used for growing large single crystals, to a batch microcrystallization format was developed by Wolff, et al. (Wolff et al., 2020). Once a slurry of satisfactory microcrystals has been obtained, one must decide how they should be delivered to the X-ray beam to be measured. Various methods are employed for this purpose, each tailored to overcome different challenges. A variety of microfluidic jets are available that create stream of liquid or other viscous medium carrying the crystals, which continuously flows through the X-ray beam (DePonte et al., 2008; Shimazu et al., 2019; Sierra et al., 2016; Vakili et al., 2020; Weierstall et al., 2014) (Fig. 5A).

Another approach is the use of fixed-target systems (Hunter et al., 2014; Lahey-Rudolph et al., 2021; Roedig et al., 2017; Zarrine-Afsar et al., 2012), where microcrystals are mounted at high density on a solid support, such as a thin film or a microfabricated chip (Gilbile et al., 2021; Roedig et al., 2015; Roedig et al., 2016; Sui et al., 2021) (Fig. 5B). With fixed-target approaches, microcrystals are positioned in an ordered array, allowing for rapid, automated data collection from each individual specimen. Acoustic droplet ejection is yet another approach, which utilizes sound waves to precisely manipulate and eject individual droplets containing crystals into the

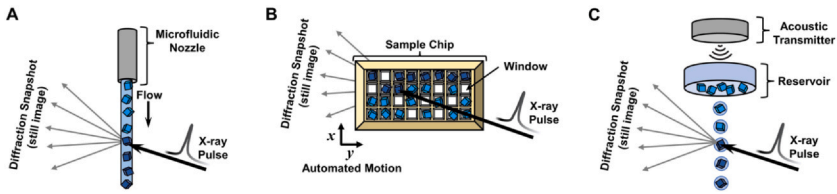

Fig. 5 Sample delivery strategies for serial crystallography. In a serial crystallography experiment, only a single diffraction image is collected from each crystal, destroying the crystal in the process and necessitating the replenishment of crystals in the beam. (A) A variety of microfluidic devices have been developed that create a freestanding liquid jet that flow crystals through the interaction region where they intersect with the (pulsed) X-ray beam. (B) Fixed-target strategies involve the deposition of hydrated crystals on some type of solid support chip, which is then rapidly translated in the horizontal and vertical directions to move crystals through the X-ray beam. (C) Acoustic methods involve the use of sound waves to eject small droplets of mother liquor containing crystals into the interaction region where they intersect with the X-ray beam. All of these methods rely on the random orientation of crystals relative to the X-ray beam. In the figure, crystals that have not yet been probed with the X-ray beam are colored bright blue, while crystals that have already been probed and are damaged are colored dark blue.

X-ray beam (Roessler et al., 2016) (Fig. 5C). A unifying feature of all these different sample delivery methods is that the many crystals measured during the experiment should be delivered to the X-ray beam in random orientations to ensure complete sampling of reciprocal space.

The second way in which serial crystallography experiments differ from standard rotation experiments relates to the data processing. In a rotation crystallography experiment, the crystal orientation only needs to be determined once, because all the images in the dataset correspond to crystal orientations that are deterministically related to one another by a known rotation about the goniometer axis. This powerful constraint is absent in serial crystallography, because every image in the data set is produced by a randomly oriented crystal. Therefore, every image must be indexed and integrated separately before merging (Boutet et al., 2012; Chapman et al., 2011). An additional problem is that because the crystals are not oscillated in the beam during the collection of individual images, full reflections are not swept through the Ewald sphere, and therefore all measurements are effectively recorded as partial intensities. This problem can be handled in several ways.

One option is to measure a large number of reflections, and simply take the mean, so that errors due to partiality average out (White, 2014). A second approach is to utilize a geometric postrefinement procedure when scaling and merging the data, which provides an estimate of the partiality of each measured reflection, and can improve the estimation of the underlying true reflection intensities (Uervirojnangkoorn et al., 2015; White, 2014). Such procedures are especially valuable when data sets only contain a modest number of images. These postrefinement procedures have their roots in the field of virus crystallography (Rossmann, Leslie, Abdel-Meguid, & Tsukihara, 1979; Winkler, Schutt, & Harrison, 1979); here, massive unit cells prohibited sizeable crystal oscillations during data collection due to the introduction of reflection overlap, resulting in a similar partiality problem.

If the X-ray source permits, the partiality problem can also be addressed by broadening the energy spectrum of the beam, creating what is known as a "pink beam" (Meents et al., 2017). When the energy spectrum of the X-ray beam is broadened, the Ewald sphere effectively becomes thicker, allowing more interaction between the sphere and reciprocal lattice points, and a better estimation of the true reflection intensity. The idiosyncrasies of processing serial crystallographic data require purpose-built computer programs that differ from the ones that are used to process data from

rotation experiments. The two primary computational tools for processing serial crystallographic data are the cctbx.xfel (Brewster et al., 2018) and CrystFEL (White, 2019) suites of programs.

3.3 Structural modeling with non-cryogenic data

In principle, modeling macromolecular structures from non-cryogenic data is no different than for cryogenic data, and identical refinement tools (Afonine et al., 2012; Murshudov et al., 2011) can be used in both cases. One notable feature of electron density maps derived from non-cryogenic experiments is that they contain fewer water molecules than those derived from cryogenic experiments (Deacon et al., 1997; Keedy et al., 2014). This observation speaks to the effect of temperature on the behavior solvent on the protein surface, which is critical for function (Fenimore, Frauenfelder, McMahon, & Parak, 2002). On the other hand, as discussed in Section 2.3, a major advantage of non-cryogenic experiments is that the resulting electron density often contains additional evidence for alternative conformations of the crystallized molecules (Fraser et al., 2009; Fraser et al., 2011).

To capitalize on this additional information, it is helpful to employ computational tools that are capable of systematically modeling alternative conformations throughout the molecule. Other Chapters within this Volume provide a detailed discussion of best practices for modeling conformational heterogeneity from crystallographic data. Therefore, this section will not discuss this topic in technical depth, but will instead simply introduce two relevant model types (Fig. 6) and tools for creating them. The first type of model is commonly referred to as a "multi-conformer" model, which has alternative conformations for some, but not all, atoms in the structure. These models can be created in an automated and systematic manner using the program qFit (Riley et al., 2021), which takes a standard model of a single protein conformation as input along with a crystallographic electron density map, and algorithmically identifies and models alternative conformations. The second type of model is an ensemble (or multi-member) model, where the entire macromolecule is represented in alternative conformations. This type of model can be generated using the PHENIX (Zwart et al., 2008) suite of software [phenix.ensemble_refinement (Burnley et al., 2012)].

A major challenge with ensemble models, and multi-conformer models to a lesser extent, is that they are prone to overfitting, because of the large number of parameters needed to represent the ensemble (Babcock, Keedy, Fraser, & Sivak, 2018). When implementing these modeling strategies, to

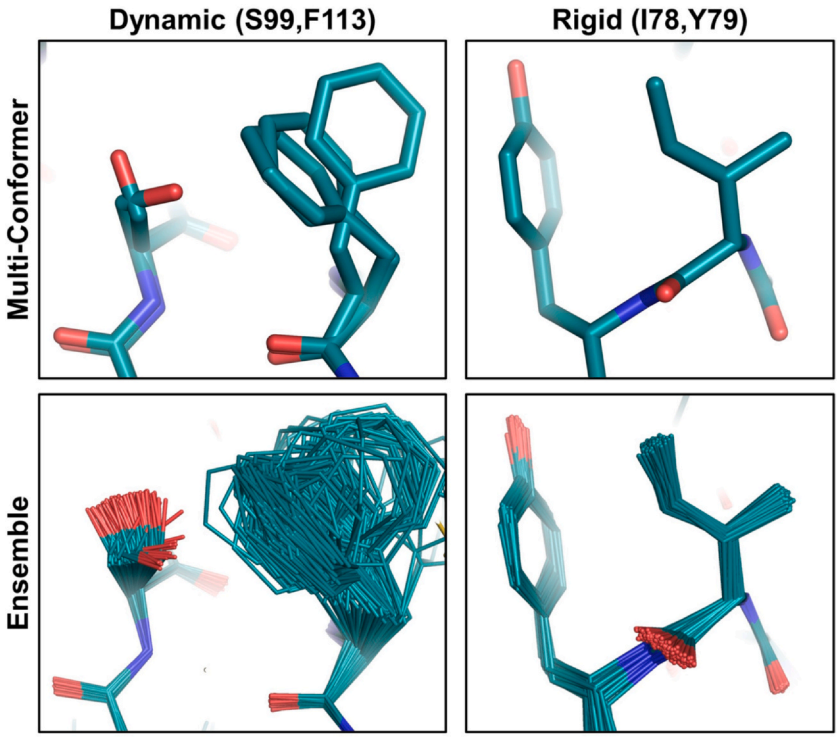

Fig. 6 Modeling conformational heterogeneity in crystal structures. The images depict the differences between two model types that are commonly used to represent conformational heterogeneity in proteins. The enzyme cyclophilin A (CypA) serves as an example, and two regions are highlighted; the sidechains of residues Ser99 and Phe113 are relatively dynamic, while the sidechains of residues Ile78 and Tyr79 are relatively rigid. The multi-conformer model (Keedy et al., 2015) includes multiple conformations for residues that display significant conformational heterogeneity, but not for residues that can be modeled well using a single conformation. On the other hand, every residue in the ensemble model (Burnley et al., 2012) contains the same number of conformations. In the case of the more dynamic residues, the side chain conformations are spread over different rotamers, whereas all the side chain conformations appear to correspond to the same rotamers for the more rigid residues.

guard against overfitting, one must watch the R-work/R-free gap as models are made increasingly complex. A recently-developed program called Vagabond also addresses the overfitting problem by reparameterizing the macromolecular structure in terms of bonds rather than atomic coordinates, and creating ensembles from deterministically related alternative conformations (Ginn, 2021).

To conclude this brief section, one might note that non-cryogenic diffraction experiments also enable the collection of diffuse scattering data, which can be used to model correlated motions of the lattice and within the crystallized molecules (Meisburger, Thomas, Watkins, & Ando, 2017; Meisburger, Case, & Ando, 2020; Meisburger, Case, & Ando, 2023; Wall, Wolff, & Fraser, 2018). This is another topic that is reviewed in great depth in other Chapters of this Volume, and therefore will only be mentioned briefly here as a potential opportunity arising from non-cryogenic macromolecular crystallography.

4. Temperature as a tool for studying conformational heterogeneity and dynamics

4.1 Multi-temperature crystallography

Temperature is a key state-variable that helps one understand the behavior of a dynamical molecular system. Specifically, when attempting to understand the behavior of a complex system, chemists and physicists have long implemented temperature perturbations to gain insight into energetics and kinetics. While this idea is commonplace in other scientific fields, it has been scarcely exploited by structural biologists attempting to understand the structures and dynamic properties of complex macromolecules, likely because the main techniques that are used to study the atomic structures of macromolecules, namely X-ray crystallography and cryoEM, have become reliant on cryocooling of samples.

The need for samples to be held in vacuum during cryoEM data collection will likely remain a prohibitive factor for performing electron microscopy at non-cryogenic temperatures; however, as described in Section 3.1, modern hardware and software developments in X-ray crystallography make non-cryogenic data collection easier than ever. This opens the door to performing high-resolution structural measurements of biological macromolecules as a function of temperature, allowing the structural biologist to explore their conformational ensembles with the tools of physical chemistry (Schmidt, Graber, Henning, & Srajer, 2010; Weik & Colletier, 2010). Experiments in which molecular structures are analyzed as a function of data collection temperature are referred to as "multi-temperature crystallography" experiments.

4.1.1 Practical considerations for multi-temperature crystallography

To perform a multi temperature crystallography experiment, a series of X-ray diffraction data sets are collected at varying temperatures. Each temperature that the investigator wishes to sample is essentially treated as an independent rotation crystallography experiment, using a separate crystal (or multiple crystals which then get merged). Because each temperature in the series is measured from a different crystal, it is important to develop a highly reproducible crystallization protocol. Additionally, care should be taken to treat all crystals the same during sample preparation in order to ensure that temperature is, in fact, the only difference between data sets in a multi-temperature series.

Many of the important practical considerations for performing multi-temperature data collection have been discussed already in this Chapter (Section 3.2). For data sets collected below 260 K, sample prep can be managed as if one is collecting "cryogenic" data, because the crystals will remain frozen during data collection. For data sets collected above 260 K, samples should be prepared for non-cryogenic data collection (see Section 3.2.1). Multi-temperature data collection requires a stable and adjustable cryojet device that can be set to maintain temperatures across the broad range of 100–300 K and higher if possible. These devices are standard at most macromolecular crystallography beamlines. Additionally, some cryojets are also equipped with a humidity stream, which offers yet another option for protecting crystals from dehydration at non-cryogenic temperatures.

An important consideration when performing multi-temperature experiments is that crystals should be equilibrated to their data collection temperatures in the cryojet stream. After mounting a crystal at ambient temperature, the crystal should be transferred to the goniometer in the cryojet stream at the desired data collection temperature. For example, if the goal is to collect data at 150 K, the experimenter should not plunge freeze the crystal in liquid nitrogen and then transfer to the diffractometer at 150 K, because then the crystal would be subjected to a cooling and warming process that other crystals (e.g. those measured at temperatures above the freezing point) did not experience. Instead, the crystal should be mounted and transferred to the diffractometer and allowed to freeze in the cryojet stream at 150 K.

This practice has a major advantage and a major drawback. The advantage is that all crystals will be subjected to the same temperature equilibration protocol, which sees them transferred from ambient temperature to data

collection temperature. The disadvantage is that the cooling rate of crystals in the cryojet stream is not as fast as in liquid cryogen, and so the crystals can be prone to developing some of the cryocooling artifacts described in Section 2.2. This can be especially problematic at intermediate temperatures, between the solvent glass transition (~200 K) and the freezing temperature of water (273 K). The problem can be mitigated by using smaller crystals that freeze faster, although this is a delicate compromise, because smaller crystals typically yield lower resolution data, and the structural modeling protocols commonly used to analyze multi-temperature experiments (see below) benefit greatly from high-resolution information. An additional strategy for improving the freezing of macromolecular crystals is slow cooling (Warkentin & Thorne, 2009).

Once crystals are successfully mounted on the goniometer and equilibrated to the data collection temperature (within seconds), the data can be collected. It is important to collect all data sets in a multi-temperature series using the same X-ray dose. This means that crystals measured at low temperatures, which may be robust to radiation damage, should receive the same dose as crystals measured at non-cryogenic temperatures. Once recorded, the data can be processed as they would for any typical rotation crystallography experiment (see Section 3.2.2).

4.1.2 Studying the conformational ensemble with multi-temperature crystallography

The idea that temperature can be used as a physical perturbation in macromolecular crystallography to probe conformational ensembles is motivated by fundamental statistical mechanics—the Boltzmann distribution dictates that increasing the temperature of a molecular ensemble will increase the population of molecules in high energy states. The first multi-temperature crystallography experiments were performed decades ago on myoglobin (Frauenfelder, Petsko, & Tsernoglou, 1979; Frauenfelder et al. 1987) and ribonuclease-A (Tilton, Dewan, & Petsko, 1992). These studies demonstrated that proteins undergo a small thermal expansion, and that B-factors also increase as a function of temperature, suggesting an increase in dynamics of the crystallized molecules.

The observed B-factor increase in these early experiments is consistent with the idea that higher energy conformational states are being additionally populated at higher temperatures. Much more recently, in 2015, Keedy, et al. reported an extremely detailed multi-temperature crystallographic study of the proline isomerase enzyme, cyclophilin A (CypA),

which demonstrated the power of the technique for mapping the conformational ensembles of proteins (Keedy et al., 2015). In this work, the authors collected eight distinct X-ray diffraction data sets across a broad range of temperatures, spanning 100–310 K. These data sets were used to algorithmically generate multi-conformer models of the enzyme with qFit (Riley et al., 2021) (see Section 3.3), which were then compared across temperatures using a composite, per-residue analysis of both B-factors and alternative conformations.

Above the solvent glass transition, most parts of CypA tended to become more heterogeneous as a function of temperature, as expected. Interestingly, the response to increasing temperature was not uniform across the enzyme, with some residues showing large increases in conformational heterogeneity, and others showing only modest increases. Additionally, there were several regions of the enzyme that appeared less dynamic with increasing temperature. This analysis yielded detailed insight into how conformational equilibria change as a function of temperature in proteins. The authors of this work also suggested that multi-conformer models derived from multi-temperature data can be used to assess which dynamic features of a protein are thermodynamically coupled to one another, by correlating their temperature-dependent behavior. Hypothetically, regions of the protein that have similar changes in heterogeneity as a function of temperature may be dynamically coupled to one another.

A powerful aspect of multi-temperature macromolecular crystallography is that it opens the door to experimental measurement of the thermodynamics that underlie observed conformational changes. When discreet alternative conformations of a macromolecule are modeled in a crystal structure and their occupancies are refined against the diffraction data, the refined occupancies give direct insight into equilibrium populations of the modeled conformations. These populations can provide estimates of equilibrium constants for conformational interconversions. Thus, for conformationally heterogeneous regions of a molecular structure, a multi-temperature crystallography experiment provides equilibrium constant information as a function of temperature.

These data can form the basis of a Van't Hoff analysis, which allows the calculation of enthalpy changes (ΔH) and entropy changes (ΔS) associated with a conformational transition, and their temperature-dependence. Although the theoretical basis for this type of analysis is valid, a detailed Van't Hoff analysis has not yet been performed using multi-temperature macromolecular crystallography data, and this represents a frontier in the field.

At present, a major limitation is likely the accuracy of occupancy values that are refined against the diffraction data. An additional frontier area of research in multi-temperature crystallography is to co-refine structures simultaneously across all temperatures, with occupancies restrained to vary smoothly across a temperature series. This type of refinement has not been performed in macromolecular crystallography; however, a related technique known as "parametric refinement" has been applied to analogous problems in materials science (Stinton & Evans, 2007). Implementing this type of refinement approach would likely enable detailed thermodynamic analysis from multi-temperature, multi-conformer models of macromolecules.

4.1.3 Examples of multi-temperature crystallography to study protein function

Multi-temperature crystallography can provide insight into the thermodynamics of a macromolecule's conformational ensemble, and this information can lead to a greater understanding of how conformational changes drive protein function. This capability is highlighted by an increasingly large body of work. In the previous section, a multi-temperature crystallographic study of CypA by Keedy, et al. (Keedy et al., 2015) was introduced, and used to describe the results that could be derived from such an experiment. Note that the observations in this study were consequential for understanding the functional mechanism of this enzyme.

In CypA, there is a network of amino acid sidechains (Arg55, Met61, Ser99, Phe113) that are known to undergo rotamer interconversions that are critical for catalytic turnover (Fraser et al., 2009). Analysis of rotamer occupancies as a function of temperature for these residues suggested that two of the four (Ser99, Phe113), which are buried deeper in the protein core, form a more tightly-coupled sub-network. This observation refined a previous model based on NMR spectroscopy, where a single exchange rate was fit to all residues in this network (Eisenmesser et al., 2005). Since 2015, several additional examples in which multi-temperature crystallography has been used to study the role of conformational heterogeneity in defining protein function have been reported. We summarize three examples here.

In 2018, in a different study, Keedy, et al. used multi-temperature crystallography to investigate allostery in protein tyrosine phosphatase 1B (Ptp1B) (Keedy et al., 2018). Ptp1B is an important drug target in diabetes (Elchebly et al., 1999) and cancer (Krishnan et al., 2014). However, most orthosteric inhibitors of Ptp1B suffer from off-target effects as a result of

inhibiting other homologs of the enzyme. In an effort to advance the design of allosteric inhibitors, the authors used multi-temperature crystallography to characterize the motion of the WPD loop, which opens and closes over the active site. Additionally, they searched for other regions of the protein that moved in concert with the WPD loop, identifying two distinct allosteric sites on the protein that were coupled to the active site. The ability of these allosteric sites, identified through multi-temperature crystallography, to perturb active site function was validated using a chemical tethering approach. This work demonstrated the potential value of multi-temperature crystallography for drug discovery.

In 2020, Otten, et al. implemented an interesting use of non-cryogenic X-ray crystallography in a study of how directed evolution reshaped the energy landscape in an enzyme to improve catalytic function (Otten et al., 2020). Specifically, the authors used crystallography and NMR to describe how successive mutations altered the conformational heterogeneity of the enzyme, to populate a narrow, highly active ensemble. This study is not a full multi-temperature series, but remarkably, the authors were able to collect crystallographic data at 70 °C (343 K). Equilibrating the crystal at this high temperature populated a hidden active conformation of the enzyme that was so sparsely occupied it could not be modeled previously. The large temperature perturbation employed in this study shows an extreme case of what is possible using temperature as a perturbation in macromolecular crystallography. Indeed, it may be possible to regularly determine crystal structures of folded proteins at temperatures that exceed their melting temperatures in solution, because the crystal lattice will provide additional stabilization to the folded structure.

In 2022, in response to the COVID-19 pandemic, Ebrahim, et al. performed a multi-temperature crystallographic study of the SARS-CoV-2 main protease (Mpro) (Ebrahim et al., 2022), with the goal of characterizing the conformational landscape and elucidating conformational states that could be targeted with novel orthosteric and allosteric inhibitors. They collected data at five temperatures spanning a range of 100–300 K, and performed a detailed analysis of conformational heterogeneity, following in the footsteps of Keedy, et al. (Keedy et al., 2015). Analysis of multi-conformer and ensemble models across the temperature series revealed coupled conformational changes across the active site, substrate-binding pocket, interdomain interface, and parts of the broad dimer interface, which offer intriguing possibilities for the design of small molecules that disrupt function by interacting with these structural elements. Additionally, in this

work the authors explored the role of relative humidity as a perturbation in addition to temperature, and found that altering humidity led to an observable change in the protein hydration shell. This idea, and its relationship to temperature perturbation was also explored by Atakisi, et al. in a study of lysozyme crystals (Atakisi, Moreau, & Thorne, 2018).

4.2 Time-resolved crystallography using temperature-jump

Electron density from multi-temperature X-ray crystallography often reveals multiple conformations of macromolecules, as described extensively above, and their occupancies represent the equilibrium populations of the observed conformational states. Experiments performed at multiple temperatures cannot reveal conformations that are not significantly populated at equilibrium, notably, the intermediate states that are transiently populated along a particular trajectory of motion (Fig. 7). Additionally, because molecular motion is very fast relative to the experimental measurement time, all kinetic information is lost, and we cannot retrieve any information about the kinematic details (dynamics) of the observed conformational changes. NMR and other spectroscopic measurements are ideal for studying the kinetics of molecular motions, but it can be difficult to correlate spectroscopic observables with the atomic details of specific conformational transitions that are observed crystallographically. Simulations

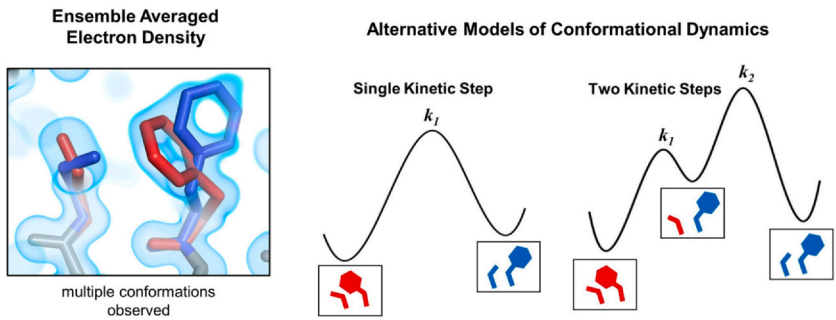

Fig. 7 Limitations of spatiotemporally-averaged electron density. This simple example shows how the electron density derived from traditional crystallographic experiments, which represents an ensemble average over space and time, is insufficient to describe the dynamics that underlie any observed conformational heterogeneity. The electron density on the left shows clear alternative conformations for the serine and phenylalanine residues shown [S99 and F113 of CypA (Fraser et al., 2009)]; however, multiple different models of conformational exchange (shown) could result in the approximately the same observed density. Time-resolved measurements have the potential ability to disambiguate these models.

can provide additional insight, but computational studies are not feasible for large systems with dynamics that occur on the microsecond to millisecond time scale.

Overcoming the challenges highlighted above, time-resolved crystallography is a powerful tool for studying functional protein motions (Moffat, 2001; Orville, 2020; Šrajer & Schmidt, 2017; Thompson et al., 2020; Wilson, 2022). This method utilizes brilliant, ultrafast X-ray pulses to provide simultaneous information about the structure and dynamics of macromolecules at high spatial and temporal resolution, thus acting like a "molecular high-speed camera." The approach allows direct measurement of structural dynamics in real time using a pump-probe strategy, where the molecules in the sample are rapidly perturbed to initiate synchronous conformational changes, and then measured at defined time delays following the perturbation to map the resulting structural changes.

A major technical bottleneck for time-resolved crystallography experiments is the need to rapidly synchronize conformational changes in the billions of molecules that constitute the sample. Historically, time-resolved crystallography has been reserved as a niche technique for studying photoactive proteins, which are easy to perturb through optical excitation of a protein-bound chromophore using a pulsed laser. The multi-temperature crystallography experiments described above (Section 4.1) demonstrate across multiple protein systems that increasing the temperature of crystallized macromolecules generally enhances populations of higher-energy conformations that are invisible at lower temperatures, suggesting temperature as viable perturbation for time-resolved measurements. Because temperature is a universal perturbation—the conformational ensembles of all complex macromolecules are sensitive to changes of this state variable—the use of rapid temperature change as a perturbation of conformational dynamics has the potential to make time-resolved crystallography a general tool for structural biology.

4.2.1 Infrared laser-induced temperature-jump

Rapid temperature change as a perturbation of chemical dynamics, known as a temperature-jump (T-jump), has been applied for decades to study chemical kinetics in a variety of different contexts (Crooks, 1983). In biochemistry, the method has been used to study protein folding (Gruebele, Sabelko, Ballew, & Ervin, 1998; Gruebele, 1999) and enzyme catalyzed reactions (Meadows, Balakrishnan, Kier, Spiro, & Klinman, 2015; Phillips et al., 2008). The idea of a T-jump centers on a temperature

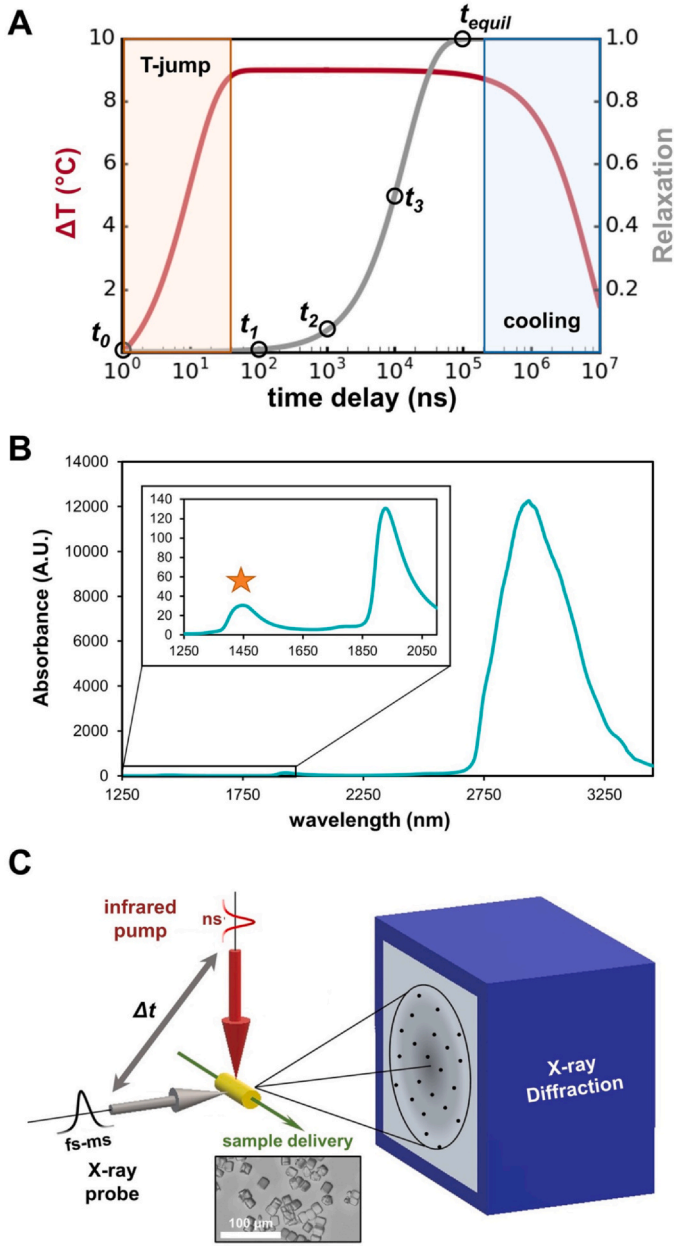

Fig. 8 Summary of T-jump crystallography. (A) In a T-jump experiment, an infrared laser pulse is used to rapidly heat an aqueous solution (red line), leading to nearly instantaneous heating, which removes any macromolecules in the solution from thermal equilibrium. On timescales that are slower than the heating pulse, the

(Continued)

change being so fast relative to the chemical process of interest that the perturbation takes the system out of thermal equilibrium, forcing it to relax to a new equilibrium (Fig. 8A). During this relaxation process, many molecules should be undergoing the same motions at roughly the same time, which allows for non-equilibrium measurements of the system. T-jumps can be introduced in a solution through excitation of molecular vibrations in the solvent molecules, which converts light energy into kinetic energy that results in a temperature increase. Because water is the common solvent for biological macromolecules, vibrational excitation of water is a universal method for increasing their temperature in solution.

Liquid water has relatively strong infrared absorbance properties, which relate to the excitation of molecular vibrations. Specifically, the absorption spectrum has peaks at approximately 1.4 and 1.9 μm, and relatively broad absorbance in the range of 2.5–4 μm (Palmer & Williams, 1974) (Fig. 8B). For most biological T-jump experiments, the absorbance peak at 1.4 μm, corresponding to the OH stretching overtone, is utilized to introduce T-jump. Absorbance at this wavelength is substantially weaker than at some other wavelengths. By utilizing another wavelength where absorbance is stronger, a larger T-jump could be achieved with the same amount of light; however, the increased absorbance would lead to a more significant temperature gradient within the sample, because the incident light intensity decreases as the beam passes through and energy is absorbed. The weaker absorbance at 1.4 μm provides an ideal compromise between the magnitude of the T-jump and attenuation through the sample.

In addition to being the correct wavelength to excite vibrations in the solvent, the incident light used for T-jump must also be delivered significantly quickly for the system to be taken out of thermal equilibrium. For studying biological macromolecules, laser sources that can deliver

Fig. 8—Cont'd macromolecules undergo conformational changes as they relax to a new thermal equilibrium (gray line), and rapid structural measurements are performed during the relaxation process (black circles). Note the logarithmic scaling of the time axis in the plot. (B) The absorbance spectrum of water (Palmer & Williams, 1974) shows several peaks in the infrared, including a large peak in the region of 2.5–3.5 μm (2500–3500 nm), and two smaller peaks centered at 1.9 μm (1900 nm) and 1.4 μm (1400 nm). The absorbance peak that is most commonly used for biological T-jump experiments is the peak at 1.4 μm (1400 nm) because it provides a good compromise between absorbance and penetration, and it is accessible with many tunable laser systems. (C) T-jump crystallography experiments are performed in a pump-probe serial format, with precise control of the delay between the infrared heating pulses and the X-ray pulses used to measure molecular structure.

several mJ of energy in 10 ns or less are ideal, because T-jumps of 10 K or more can typically be achieved and the duration of the heating pulse is faster than many functional motions, which take place in the microsecond to millisecond time scale. Additionally, because thermal equilibration of molecules typically occurs on the order of picoseconds (Rubtsov & Burin, 2019), one assumes that sample heating is homogenous over the duration of the nanosecond laser pulse. This assumption holds true for crystalline macromolecules as well, because their crystals tend to have large channels that are permeated with bulk solvent that also undergoes infrared irradiation and experiences a T-jump.

4.2.2 Practical considerations for T-jump crystallography experiments

Infrared laser-induced T-jump can be utilized as a rapid perturbation for time-resolved crystallography measurements of macromolecular structural dynamics (Wolff et al., 2022). T-jump crystallography experiments occur in a unique pump-probe format (Fig. 8C) that relies on the use of serial crystallography (see Section 3.2.3). In the serial crystallography experiment, a single X-ray diffraction snapshot is measured from each of many crystals using an X-ray pulse. To incorporate the T-jump, a pulsed infrared laser tuned to a wavelength of approximately 1.4 μm is focused on the "interaction region" where X-rays impinge on the sample. The laser pulses rapidly heat microcrystals as they pass through the interaction region (in either a microfluidic or fixed-target format, see Section 3.2.3), and the timing of infrared and X-ray pulses is coordinated so that the heating occurs at a defined time delay prior to structural measurement with an X-ray pulse. The heating is effectively instantaneous (typically nanoseconds, depending on the laser source) relative to slower (microsecond to millisecond) molecular motions, and the macromolecules are removed from thermal equilibrium. By sampling multiple pump-probe time delays, it is possible to map both the spatial and temporal details (structure and kinetics) of molecular motion.

An important aspect of this experiment is that it requires the ability to generate suitable X-ray pulses, which is only possible at XFEL sources or specialized synchrotron beamlines (Cammarata et al., 2009; Graber et al., 2011). The temporal resolution of the experiment is limited by the duration of either the pump (infrared) or probe (X-ray) pulses, whichever is longer in duration. Alternatively, time-resolved experiments can be performed without a pulsed X-ray source, if a fast frame rate detector is

available (Singh et al., 2013). In this case, the temporal resolution is set by the detector frame rate.

There are several critical aspects of the experimental setup described above that must be considered carefully when designing a T-jump crystallography experiment. First, because the T-jump relies on the presence of water, crystals should be prepared for serial crystallography in an aqueous solution or carrier medium. If high sample viscosity is desired, hydroxyethyl cellulose is an ideal material (Sugahara et al., 2017), because it is aqueous and does not undergo unusual phase transitions like many of its hydrophobic counterparts including LCP (Czeslik, Winter, Rapp, & Bartels, 1995). Next, the properties of the infrared pump laser are crucial for success. The role of the wavelength in creating a uniform temperature jump and of the pulse duration in defining the temporal resolution of the experiment have already been mentioned. Additionally, the overall fluence (mJ/mm^2) of the infrared beam determines the magnitude of the T-jump that is introduced in the sample. High fluence at the sample can be achieved by producing many photons per pulse (high pulse energy), and/or by focusing the beam to a smaller area. Special cameras that are sensitive to the mid-infrared region of the electromagnetic spectrum are also critical for aligning the pump and probe beams with one another and with the sample.

A major question when performing T-jump experiments relates to the instantaneous temperature of the sample during the X-ray measurement. Fortunately, samples of macromolecules contain a sensitive internal thermometer, because the X-ray scattering of liquid water is highly sensitive to temperature. By analyzing the radial average of the solvent scattering background that is present in the diffraction images, it is possible to detect the presence or absence of a temperature jump, and in favorable cases, to estimate its magnitude (Cammarata et al., 2006; Cho et al., 2018; Thompson et al., 2019; Wolff et al., 2022).

The ability to use the solvent scattering signal as a proxy for temperature also allows the experimenter to monitor the system for cooling. In a T-jump experiment, the longest pump-probe time delays that can be sampled are limited by sample cooling, so it is valuable to have a reliable estimate of when the effect becomes limiting. Empirically, using current experimental setups, the longest possible pump-probe time delays that can be achieved are hundreds of microseconds (Thompson et al., 2019). As of this writing, T-jump crystallography is a new technique, and one might note that new hardware and software to facilitate these experiments are in rapid development.

Extracting meaningful structural changes from the results of a time-resolved crystallography experiment can be challenging, and this is especially true for T-jump experiments. Typically, the modest T-jumps that can be practically introduced only shift the populations of conformational states by a very small amount. Therefore, direct refinement of atomic coordinates against structure factor data in the presence and absence of a T-jump will likely produce identical models. In order to isolate the time-resolved signals that arise from the T-jump, it is necessary to analyze difference structure factors and difference electron density maps calculated between data measured with and without introduction of a T-jump. Difference electron density is sensitive to subtle differences between the underlying structure factors, and the small signals that represent protein motions are visible in time-resolved difference maps (Ursby & Bourgeois, 1997). Time-resolved difference density can be quantified for direct analysis (Wickstrand et al., 2020), or it can be used to create structural models of high-energy conformational states that can be refined against the raw or extrapolated structure factor data (De Zitter, Coquelle, Oeser, Barends, & Colletier, 2022), analysis methods that have become commonplace in time-resolved crystallography. It is worth noting that T-jump generally leads to widespread structural changes throughout the unit cell, which can be problematic for structure factor extrapolation methods that rely on scalar approximations (Genick, 2007), so this method should be approached with caution for T-jump experiments.

4.2.3 Studying macromolecular dynamics with T-jump

T-jump has only recently been combined with X-ray scattering to be used as a tool for structural biology. Consequently, there are only limited examples of its use, and they will be reviewed briefly here. The majority of time-resolved T-jump X-ray experiments in structural biology (3/4) have been performed using small- and wide-angle X-ray scattering (SAXS/WAXS) as a probe, rather than crystallography.

The first proof-of-principle that T-jump could be combined with X-ray scattering to study macromolecular dynamics came from a series of papers published by Rimmerman and coworkers (Rimmerman et al., 2017, 2018). In this work, the authors used T-jump to induce changes in insulin oligomerization state paired with SAXS/WAXS to follow the dynamics from nanoseconds to milliseconds. Analysis of the time-resolved scattering curves by singular value decomposition (SVD) revealed several transient intermediates involved in the association and dissociation of oligomers.

Later in 2018, Cho, et al. also performed T-jump SAXS/WAXS on the R-state of tetrameric hemoglobin, to study the effect of R-state heterogeneity on the transition from the R-state to the T-state (Cho et al., 2018). In 2019, Thompson et al. again used T-jump paired with SAXS/WAXS to study the internal dynamics of the enzyme cyclophilin A (CypA) (Thompson et al., 2019). In this work, two distinct functional motions could be mapped, one corresponding to catalysis and the other to substrate recognition. Importantly, in this study, mutants of the enzyme that are known to have altered catalytic and substrate binding functions were used as controls to confirm the functional relevance of the observed time-resolved signals.

More recently, Wolff and coworkers demonstrated the first application of T-jump to time-resolved macromolecular crystallography (Wolff et al., 2022). Here the authors used microcrystals of the enzyme lysozyme in a pump-probe serial T-jump crystallography experiment, as described in detail above (Section 4.2.2). The authors measured data corresponding to 20 ns, 20 μs, and 200 μs pump-probe time delays. Analysis of time-resolved difference electron density maps revealed signals related to heating of the enzyme, manifesting as increased harmonic motions (B-factors) and side chain rotations at 20 ns after the introduction of T-jump, followed by dissipation of those short amplitude motions into larger, correlated loop motions at longer pump-probe time delays. These larger amplitude motions, which appeared to be involved in the well-known hinge-bending motion of lysozyme (Mccammon, Gelin, Karplus, & Wolynes, 1976), could be included in multi-conformer models and refined against the time-resolved data. Similar to the SAXS/WAXS experiments by Thompson, et al. (Thompson et al., 2019), the T-jump crystallography study by Wolff, et al. included an important functional control. T-jump crystallography experiments were repeated in the presence of chitobiose, an enzyme inhibitor that arrests the hinge-bending motion of lysozyme. In the presence of chitobiose, the time-resolved signals do not dissipate in the same manner as they do for the apo enzyme, which corroborated the connection between the time-resolved signal changes and the hinge-bending motion of the enzyme.

5. Conclusion

Temperature is a key variable that governs the dynamic behavior of complex macromolecules, but it has been underutilized as a tool for structural biology. Given the traditional reliance of high-resolution structural techniques

on sample cryocooling, this is somewhat unsurprising. Fortunately, modern advances in X-ray crystallography eliminate the need for cryocooling in many cases. Using sensitive detectors and modern data-processing software, it is possible to collect high-resolution X-ray diffraction with a very low X-ray dose, mitigating the ill effects of radiation damage. The ability to collect diffraction data near ambient/physiological temperature eliminates artifacts that are associated with cryocooling, and enables the use of temperature as a perturbation to study structure and dynamics using multi-temperature and time-resolved T-jump crystallography. Experiments that integrate temperature perturbations with high-resolution X-ray crystallography can provide detailed insight into the correlated motions that drive the functions of biological macromolecules.

References

Afonine, P. V., Grosse-Kunstleve, R. W., Echols, N., Headd, J. J., Moriarty, N. W., Mustyakimov, M., ... Adams, P. D. (2012). Towards automated crystallographic structure refinement with phenix.refine. *Acta Crystallographica. Section D, Biological Crystallography, 68*(Pt 4), 352–367. https://doi.org/10.1107/S0907444912001308.

Amemiya, Y. (2008). Imaging plate - X-ray area detector based on photostimulable phosphor. *Synchrotron Radiation News, 3*, 21–26. https://doi.org/10.1080/08940889008602552.

Atakisi, H., Moreau, D. W., & Thorne, R. E. (2018). Effects of protein-crystal hydration and temperature on side-chain conformational heterogeneity in monoclinic lysozyme crystals. *Acta Crystallographica. Section D, Structural Biology, 74*(Pt 4), 264–278. https://doi.org/10.1107/S2059798318000207.

Baba, S., Hoshino, T., Ito, L., & Kumasaka, T. (2013). Humidity control and hydrophilic glue coating applied to mounted protein crystals improves X-ray diffraction experiments. *Acta Crystallographica. Section D, Biological Crystallography, 69*(Pt 9), 1839–1849. https://doi.org/10.1107/S0907444913018027.

Babcock, N. S., Keedy, D. A., Fraser, J. S., & Sivak, D. A. (2018). Model selection for biological crystallography. *bioRxiv*. 448795. ⟨https://doi.org/10.1101/448795⟩.

Baxter, E. L., Aguila, L., Alonso-Mori, R., Barnes, C. O., Bonagura, C. A., Brehmer, W., ... Cohen, A. E. (2016). High-density grids for efficient data collection from multiple crystals. *Acta Crystallographica. Section D, Structural Biology, 72*(1), 1. https://doi.org/10.1107/S2059798315020847.

Boutet, S., Lomb, L., Williams, G. J., Barends, T. R. M., Aquila, A., Doak, R. B., ... Schlichting, I. (2012). High-resolution protein structure determination by serial femtosecond crystallography. *Science (New York, N. Y.), 337*(6092), 362–364. https://doi.org/10.1126/science.1217737.

Brewster, A. S., Waterman, D. G., Parkhurst, J. M., Gildea, R. J., Young, I. D., O'Riordan, L. J., ... Sauter, N. K. (2018). Improving signal strength in serial crystallography with DIALS geometry refinement. *Acta Crystallographica. Section D, Structural Biology, 74*(9), 9. https://doi.org/10.1107/S2059798318009191.

Burnley, B. T., Afonine, P. V., Adams, P. D., & Gros, P. (2012). Modelling dynamics in protein crystal structures by ensemble refinement. *ELife, 1*, e00311. https://doi.org/10.7554/eLife.00311.

Bury, C. S., Brooks-Bartlett, J. C., Walsh, S. P., & Garman, E. F. (2018). Estimate your dose: RADDOSE-3D. *Protein Science: A Publication of the Protein Society, 27*(1), 217–228. https://doi.org/10.1002/pro.3302.

Cammarata, M., Eybert, L., Ewald, F., Reichenbach, W., Wulff, M., Anfinrud, P., ... Polachowski, S. (2009). Chopper system for time resolved experiments with synchrotron radiation. *The Review of Scientific Instruments, 80*(1), 015101. https://doi.org/10.1063/1.3036983.

Cammarata, M., Lorenc, M., Kim, T. K., Lee, J. H., Kong, Q. Y., Pontecorvo, E., ... Ihee, H. (2006). Impulsive solvent heating probed by picosecond x-ray diffraction. *The Journal of Chemical Physics, 124*(12), 124504. https://doi.org/10.1063/1.2176617.

Chapman, H. N., Fromme, P., Barty, A., White, T. A., Kirian, R. A., Aquila, A., ... Spence, J. C. H. (2011). Femtosecond X-ray protein nanocrystallography. *Nature, 470*(7332), 73–77. https://doi.org/10.1038/nature09750.

Cho, H. S., Schotte, F., Stadnytskyi, V., DiChiara, A., Henning, R., & Anfinrud, P. (2018). Dynamics of quaternary structure transitions in R-state carbonmonoxyhemoglobin unveiled in time-resolved X-ray scattering patterns following a temperature jump. *The Journal of Physical Chemistry. B, 122*(49), 11488–11496. https://doi.org/10.1021/acs.jpcb.8b07414.

Crooks, J. E. (1983). The temperature-jump technique for the study of fast reactions in solution. *Journal of Physics E: Scientific Instruments, 16*(12), 1142–1147. https://doi.org/10.1088/0022-3735/16/12/003.

Czeslik, C., Winter, R., Rapp, G., & Bartels, K. (1995). Temperature- and pressure-dependent phase behavior of monoacylglycerides monoolein and monoelaidin. *Biophysical Journal, 68*(4), 1423–1429. https://doi.org/10.1016/S0006-3495(95)80315-2.

De La Mora, E., Coquelle, N., Bury, C. S., Rosenthal, M., Holton, J. M., Carmichael, I., ... Weik, M. (2020). Radiation damage and dose limits in serial synchrotron crystallography at cryo- and room temperatures. *Proceedings of the National Academy of Sciences of the United States of America, 117*(8), 4142–4151. https://doi.org/10.1073/pnas.1821522117.

De Zitter, E., Coquelle, N., Oeser, P., Barends, T. R. M., & Colletier, J.-P. (2022). Xtrapol8 enables automatic elucidation of low-occupancy intermediate-states in crystallographic studies. *Communications Biology, 5*(1), 1. https://doi.org/10.1038/s42003-022-03575-7.

Deacon, A., Gleichmann, T., Kalb (Gilboa), A. J., Price, H., Raftery, J., Bradbrook, G., ... Helliwell, J. R. (1997). The structure of concanavalin A and its bound solvent determined with small-molecule accuracy at 0.94 [Aring]resolution. *Journal of the Chemical Society, Faraday Transactions, 93*(24), 4305–4312. https://doi.org/10.1039/A704140C.

DePonte, D. P., Weierstall, U., Schmidt, K., Warner, J., Starodub, D., Spence, J. C. H., & Doak, R. B. (2008). Gas dynamic virtual nozzle for generation of microscopic droplet streams. *Journal of Physics D: Applied Physics, 41*(19), 195505. https://doi.org/10.1088/0022-3727/41/19/195505.

Diamond, R. (1969). Profile analysis in single crystal diffractometry. *Acta Crystallographica. Section A, Crystal Physics, Diffraction, Theoretical and General Crystallography, 25*(1), 43–55. https://doi.org/10.1107/s0567739469000064.

Dobrianov, I., Caylor, C., Lemay, S. G., Finkelstein, K. D., & Thorne, R. E. (1999). X-ray diffraction studies of protein crystal disorder. *Journal of Crystal Growth, 196*(2), 511–523. https://doi.org/10.1016/S0022-0248(98)00833-1.

Ebrahim, A., Riley, B. T., Kumaran, D., Andi, B., Fuchs, M. R., McSweeney, S., & Keedy, D. A. (2022). The temperature-dependent conformational ensemble of SARS-CoV-2 main protease (Mpro). *IUCrJ, 9*(5), 5. https://doi.org/10.1107/S2052252522007497.

Eisenmesser, E. Z., Millet, O., Labeikovsky, W., Korzhnev, D. M., Wolf-Watz, M., Bosco, D. A., ... Kern, D. (2005). Intrinsic dynamics of an enzyme underlies catalysis. *Nature, 438*(7064), 117–121. https://doi.org/10.1038/nature04105.

Elchebly, M., Payette, P., Michaliszyn, E., Cromlish, W., Collins, S., Loy, A. L., ... Kennedy, B. P. (1999). Increased insulin sensitivity and obesity resistance in mice lacking the protein tyrosine phosphatase-1B gene. *Science (New York, N. Y.), 283*(5407), 1544–1548. https://doi.org/10.1126/science.283.5407.1544.

Evans, G., Axford, D., & Owen, R. L. (2011). The design of macromolecular crystallography diffraction experiments. *Acta Crystallographica. Section D, Biological Crystallography, 67*(4), 261–270. https://doi.org/10.1107/S0907444911007608.

Evans, P. (2006). Scaling and assessment of data quality. *Acta Crystallographica. Section D, Biological Crystallography, 62*(Pt 1), 72–82. https://doi.org/10.1107/S0907444905036693.

Fenimore, P. W., Frauenfelder, H., Magazù, S., McMahon, B. H., Mezei, F., Migliardo, F., ... Stroe, I. (2013). Concepts and problems in protein dynamics. *Chemical Physics, 424*, 2–6. https://doi.org/10.1016/j.chemphys.2013.06.023.

Fenimore, P. W., Frauenfelder, H., McMahon, B. H., & Parak, F. G. (2002). Slaving: Solvent fluctuations dominate protein dynamics and functions. *Proceedings of the National Academy of Sciences of the United States of America, 99*(25), 16047–16051. https://doi.org/10.1073/pnas.212637899.

First Analysis of Macromolecular Crystals | Springer Nature Experiments. (n.d.). Retrieved June 1, 2023, from ⟨https://experiments.springernature.com/articles/10.1385/1–59745-266–1:43⟩.

Fischer, M., Shoichet, B. K., & Fraser, J. S. (2015). One crystal, two temperatures: Cryocooling penalties alter ligand binding to transient protein sites. *Chembiochem: A European Journal of Chemical Biology, 16*(11), 1560–1564. https://doi.org/10.1002/cbic.201500196.

Foadi, J., Aller, P., Alguel, Y., Cameron, A., Axford, D., Owen, R. L., ... Evans, G. (2013). Clustering procedures for the optimal selection of data sets from multiple crystals in macromolecular crystallography. *Acta Crystallographica Section D: Biological Crystallography, 69*(8), 1617–1632. https://doi.org/10.1107/S0907444913012274.

Förster, A., Brandstetter, S., & Schulze-Briese, C. (2019). Transforming X-ray detection with hybrid photon counting detectors. *Philosophical Transactions of the Royal Society A: Mathematical, Physical and Engineering Sciences, 377*(2147), 20180241. https://doi.org/10.1098/rsta.2018.0241.

Fraser, J. S., Clarkson, M. W., Degnan, S. C., Erion, R., Kern, D., & Alber, T. (2009). Hidden alternative structures of proline isomerase essential for catalysis. *Nature, 462*(7273), 669–673. https://doi.org/10.1038/nature08615.

Fraser, J. S., Van Den Bedem, H., Samelson, A. J., Lang, P. T., Holton, J. M., Echols, N., & Alber, T. (2011). Accessing protein conformational ensembles using room-temperature X-ray crystallography. *Proceedings of the National Academy of Sciences of the United States of America, 108*(39), 16247–16252. https://doi.org/10.1073/pnas.1111325108.

Frauenfelder, H., Chen, G., Berendzen, J., Fenimore, P. W., Jansson, H., McMahon, B. H., ... Young, R. D. (2009). A unified model of protein dynamics. *Proceedings of the National Academy of Sciences of the United States of America, 106*(13), 5129–5134. https://doi.org/10.1073/pnas.0900336106.

Frauenfelder, H., Hartmann, H., Karplus, M., Kuntz, I. D., Kuriyan, J., Parak, F., ... Connolly, M. L. (1987). Thermal expansion of a protein. *Biochemistry, 26*(1), 254–261. https://doi.org/10.1021/bi00375a035.

Frauenfelder, H., Petsko, G. A., & Tsernoglou, D. (1979). Temperature-dependent X-ray diffraction as a probe of protein structural dynamics. *Nature, 280*(5723), 558–563. https://doi.org/10.1038/280558a0.

Fuchs, M. R., Pradervand, C., Thominet, V., Schneider, R., Panepucci, E., Grunder, M., ... Wang, M. (2014). D3, the new diffractometer for the macromolecular crystallography beamlines of the Swiss Light Source. *Journal of Synchrotron Radiation, 21*(Pt 2), 340–351. https://doi.org/10.1107/S160057751400006X.

Gallagher-Jones, M., Bastillo, K. C., Ophus, C., Richards, L. S., Ciston, J., Lee, S., ... Rodriguez, J. A. (2020). Atomic structures determined from digitally defined nanocrystalline regions. *IUCrJ, 7*(3), 490–499. https://doi.org/10.1107/S2052252520004030.

Garman, E. (2003). "Cool" crystals: Macromolecular cryocrystallography and radiation damage. *Current Opinion in Structural Biology, 13*(5), 545–551. https://doi.org/10.1016/j.sbi.2003.09.013.

Garman, E. F., & Weik, M. (2017). Radiation damage in macromolecular crystallography. *Methods in Molecular Biology (Clifton, N. J.), 1607*, 467–489. https://doi.org/10.1007/978-1-4939-7000-1_20.

Genick, U. K. (2007). Structure-factor extrapolation using the scalar approximation: Theory, applications and limitations. *Acta Crystallographica. Section D, Biological Crystallography, 63*(Pt 10), 1029–1041. https://doi.org/10.1107/S0907444907038164.

Gilbile, D., Shelby, M. L., Lyubimov, A. Y., Wierman, J. L., Monteiro, D. C. F., Cohen, A. E., ... Kuhl, T. L. (2021). Plug-and-play polymer microfluidic chips for hydrated, room temperature, fixed-target serial crystallography. *Lab on a Chip, 21*(24), 4831–4845. https://doi.org/10.1039/D1LC00810B.

Gildea, R. J., Beilsten-Edmands, J., Axford, D., Horrell, S., Aller, P., Sandy, J., ... Winter, G. (2022). xia2.multiplex: A multi-crystal data-analysis pipeline. *Acta Crystallographica. Section D, Structural Biology, 78*(6), 752–769. https://doi.org/10.1107/S2059798322004399.

Ginn, H. M. (2021). Vagabond: Bond-based parametrization reduces overfitting for refinement of proteins. *Acta Crystallographica. Section D, Structural Biology*, 77(4), 4. https://doi.org/10.1107/S2059798321000826.

Graber, T., Anderson, S., Brewer, H., Chen, Y. S., Cho, H. S., Dashdorj, N., ... Moffat, K. (2011). BioCARS: A synchrotron resource for time-resolved X-ray science. *Journal of Synchrotron Radiation, 18*(Pt 4), 658–670. https://doi.org/10.1107/S0909049511009423.

Gruebele, M. (1999). The fast protein folding problem. *Annual Review of Physical Chemistry, 50*(1), 485–516. https://doi.org/10.1146/annurev.physchem.50.1.485.

Gruebele, M., Sabelko, J., Ballew, R., & Ervin, J. (1998). Laser temperature jump induced protein refolding. *Accounts of Chemical Research, 31*(11), 699–707. https://doi.org/10.1021/ar970083x.

Gruner, S. M., Eikenberry, E. F., & Tate, M. W. (2006). *Comparison of X-ray detectors* [Text]. Urn:Isbn:978–0-7923–6857-1; International Union of Crystallography. ⟨https://doi.org/10.1107/97809553602060000667⟩.

Gruner, S. M., & Lattman, E. E. (2015). Biostructural science inspired by next-generation X-ray sources. *Annual Review of Biophysics, 44*, 33–51. https://doi.org/10.1146/annurev-biophys-060414-033813.

Haas, D. J. (2020). The early history of cryo-cooling for macromolecular crystallography. *IUCrJ, 7*(Pt 2), 148–157. https://doi.org/10.1107/S2052252519016993.

Halle, B. (2004). Biomolecular cryocrystallography: Structural changes during flash-cooling. *Proceedings of the National Academy of Sciences, 101*(14), 4793–4798. https://doi.org/10.1073/pnas.0308315101.

Hargreaves, D. (2012). A manual low-cost protein-crystallization plate jig for in situ diffraction in the home laboratory. *Journal of Applied Crystallography, 45*(Pt 1), 138–140. https://doi.org/10.1107/S0021889811052654.

Henzler-Wildman, K., & Kern, D. (2007). Dynamic personalities of proteins. *Nature, 450*(7172), 964–972. https://doi.org/10.1038/nature06522.

Holton, J. M. (2009). A beginner's guide to radiation damage. *Journal of Synchrotron Radiation, 16*(Pt 2), 133–142. https://doi.org/10.1107/S0909049509004361.

Hunter, M. S., Segelke, B., Messerschmidt, M., Williams, G. J., Zatsepin, N. A., Barty, A., ... Frank, M. (2014). Fixed-target protein serial microcrystallography with an x-ray free electron laser. *Scientific Reports, 4*(1), 1. https://doi.org/10.1038/srep06026.

Juers, D. H., & Matthews, B. W. (2001). Reversible lattice repacking illustrates the temperature dependence of macromolecular interactions. *Journal of Molecular Biology, 311*(4), 851–862. https://doi.org/10.1006/jmbi.2001.4891.

Juers, D. H., & Matthews, B. W. (2004a). Cryo-cooling in macromolecular crystallography: Advantages, disadvantages and optimization. *Quarterly Reviews of Biophysics, 37*(2), 105–119. https://doi.org/10.1017/s0033583504004007.

Juers, D. H., & Matthews, B. W. (2004b). The role of solvent transport in cryo-annealing of macromolecular crystals. *Acta Crystallographica. Section D, Biological Crystallography, 60*(Pt 3), 412–421. https://doi.org/10.1107/S0907444903027938.

Kabsch, W. (2010). XDS. *Acta Crystallographica. Section D, Biological Crystallography, 66*(Pt 2), 125–132. https://doi.org/10.1107/S0907444909047337.

Karplus, P. A., & Diederichs, K. (2012). Linking crystallographic model and data quality. *Science (New York, N. Y.), 336*(6084), 1030–1033. https://doi.org/10.1126/science.1218231.

Keedy, D. A., Hill, Z. B., Biel, J. T., Kang, E., Rettenmaier, T. J., Brandão-Neto, J., ... Fraser, J. S. (2018). An expanded allosteric network in PTP1B by multitemperature crystallography, fragment screening, and covalent tethering. *ELife,* 7, e36307. https://doi.org/10.7554/eLife.36307.

Keedy, D. A., Kenner, L. R., Warkentin, M., Woldeyes, R. A., Hopkins, J. B., Thompson, M. C., ... Fraser, J. S. (2015). Mapping the conformational landscape of a dynamic enzyme by multitemperature and XFEL crystallography. *ELife, 4*, e07574. https://doi.org/10.7554/eLife.07574.

Keedy, D. A., Van Den Bedem, H., Sivak, D. A., Petsko, G. A., Ringe, D., Wilson, M. A., & Fraser, J. S. (2014). Crystal cryocooling distorts conformational heterogeneity in a model Michaelis complex of DHFR. *Structure (London, England: 1993), 22*(6), 899–910. https://doi.org/10.1016/j.str.2014.04.016.

Kriminski, S., Caylor, C. L., Nonato, M. C., Finkelstein, K. D., & Thorne, R. E. (2002). Flash-cooling and annealing of protein crystals. *Acta Crystallographica. Section D, Biological Crystallography, 58*(3), 3. https://doi.org/10.1107/S0907444902000112.

Kriminski, S., Kazmierczak, M., & Thorne, R. E. (2003). Heat transfer from protein crystals: Implications for flash-cooling and X-ray beam heating. *Acta Crystallographica. Section D, 59*(4), 697–708. https://doi.org/10.1107/S0907444903002713.

Krishnan, N., Koveal, D., Miller, D. H., Xue, B., Akshinthala, S. D., Kragelj, J., ... Tonks, N. K. (2014). Targeting the disordered C terminus of PTP1B with an allosteric inhibitor. *Nature Chemical Biology, 10*(7), 558–566. https://doi.org/10.1038/nchembio.1528.

Lahey-Rudolph, J. M., Schönherr, R., Barthelmess, M., Fischer, P., Seuring, C., Wagner, A., ... Redecke, L. (2021). Fixed-target serial femtosecond crystallography using in cellulo grown microcrystals. *IUCrJ, 8*(Pt 4), 665–677. https://doi.org/10.1107/S2052252521005297.

Lang, P. T., Ng, H.-L., Fraser, J. S., Corn, J. E., Echols, N., Sales, M., ... Alber, T. (2010). Automated electron-density sampling reveals widespread conformational polymorphism in proteins. *Protein Science: A Publication of the Protein Society, 19*(7), 1420–1431. https://doi.org/10.1002/pro.423.

López-Jaramillo, F. J., Moraleda, A. B., González-Ramírez, L. A., Carazo, A., & García-Ruiz, J. M. (2002). Soaking: The effect of osmotic shock on tetragonal lysozyme crystals. *Acta Crystallographica. Section D, Biological Crystallography, 58*(Pt 2), 209–214. https://doi.org/10.1107/s090744490101914x.

Lyubimov, A. Y., Murray, T. D., Koehl, A., Araci, I. E., Uervirojnangkoorn, M., Zeldin, O. B., ... Berger, J. M. (2015). Capture and X-ray diffraction studies of protein microcrystals in a microfluidic trap array. *Acta Crystallographica. Section D, Biological Crystallography, 71*(Pt 4), 928–940. https://doi.org/10.1107/S1399004715002308.

Martin-Garcia, J. M., Conrad, C. E., Nelson, G., Stander, N., Zatsepin, N. A., Zook, J., ... Liu, W. (2017). Serial millisecond crystallography of membrane and soluble protein microcrystals using synchrotron radiation. *IUCrJ, 4*(4), 439–454. https://doi.org/10.1107/S205225251700570X.

Mccammon, J. A., Gelin, B. R., Karplus, M., & Wolynes, P. G. (1976). The hinge-bending mode in lysozyme. *Nature, 262*(5566), 5566. https://doi.org/10.1038/262325a0.

Meadows, C. W., Balakrishnan, G., Kier, B. L., Spiro, T. G., & Klinman, J. P. (2015). Temperature-jump fluorescence provides evidence for fully reversible microsecond

dynamics in a thermophilic alcohol dehydrogenase. *Journal of the American Chemical Society, 137*(32), 10060–10063. https://doi.org/10.1021/jacs.5b04413.

Meents, A., Wiedorn, M. O., Srajer, V., Henning, R., Sarrou, I., Bergtholdt, J., ... Chapman, H. N. (2017). Pink-beam serial crystallography. *Nature Communications, 8*(1), 1. https://doi.org/10.1038/s41467-017-01417-3.

Mehrabi, P., Bücker, R., Bourenkov, G., Ginn, H. M., von Stetten, D., Müller-Werkmeister, H. M., ... Miller, R. J. D. (2021). Serial femtosecond and serial synchrotron crystallography can yield data of equivalent quality: A systematic comparison. *Science Advances,* 7(12), eabf1380. https://doi.org/10.1126/sciadv.abf1380.

Meisburger, S. P., Case, D. A., & Ando, N. (2020). Diffuse X-ray scattering from correlated motions in a protein crystal. *Nature Communications, 11*(1), 1271. https://doi.org/10.1038/s41467-020-14933-6.

Meisburger, S. P., Case, D. A., & Ando, N. (2023). Robust total X-ray scattering workflow to study correlated motion of proteins in crystals. *Nature Communications, 14*(1), 1. https://doi.org/10.1038/s41467-023-36734-3.

Meisburger, S. P., Thomas, W. C., Watkins, M. B., & Ando, N. (2017). X-ray scattering studies of protein structural dynamics. *Chemical Reviews, 117*(12), 7615–7672. https://doi.org/10.1021/acs.chemrev.6b00790.

Moffat, K. (2001). Time-resolved biochemical crystallography: A mechanistic perspective. *Chemical Reviews, 101*(6), 1569–1582. https://doi.org/10.1021/cr990039q.

Moreau, D. W., Atakisi, H., & Thorne, R. E. (2019). Solvent flows, conformation changes and lattice reordering in a cold protein crystal. *Acta Crystallographica. Section D, Structural Biology,* 75(11), 11. https://doi.org/10.1107/S2059798319013822.

Moreau, D. W., Atakisi, H., & Thorne, R. E. (2021). Ice in biomolecular cryocrystallography. *Acta Crystallographica. Section D, Structural Biology,* 77(4), 4. https://doi.org/10.1107/S2059798321001170.

Murray, T. D., Lyubimov, A. Y., Ogata, C. M., Vo, H., Uervirojnangkoorn, M., Brunger, A. T., & Berger, J. M. (2015). A high-transparency, micro-patternable chip for X-ray diffraction analysis of microcrystals under native growth conditions. *Acta Crystallographica. Section D, Biological Crystallography, 71*(Pt 10), 1987–1997. https://doi.org/10.1107/S1399004715015011.

Murshudov, G. N., Skubák, P., Lebedev, A. A., Pannu, N. S., Steiner, R. A., Nicholls, R. A., ... Vagin, A. A. (2011). REFMAC5 for the refinement of macromolecular crystal structures. *Acta Crystallographica Section D: Biological Crystallography, 67*(4), 4. https://doi.org/10.1107/S0907444911001314.

Nam, K. H., Kim, J., & Cho, Y. (2021). Polyimide mesh-based sample holder with irregular crystal mounting holes for fixed-target serial crystallography. *Scientific Reports, 11*(1), 1. https://doi.org/10.1038/s41598-021-92687-x.

Nave, C., & Garman, E. F. (2005). Towards an understanding of radiation damage in cryocooled macromolecular crystals. *Journal of Synchrotron Radiation, 12*(Pt 3), 257–260. https://doi.org/10.1107/S0909049505007132.

Okumura, H., Sakai, N., Murakami, H., Mizuno, N., Nakamura, Y., Ueno, G., ... Kumasaka, T. (2022). In situ crystal data-collection and ligand-screening system at SPring-8. *Acta Crystallographica. Section F, Structural Biology Communications, 78*(Pt 6), 241–251. https://doi.org/10.1107/S2053230X22005283.

Orville, A. M. (2020). Recent results in time resolved serial femtosecond crystallography at XFELs. *Current Opinion in Structural Biology, 65*, 193–208. https://doi.org/10.1016/j.sbi.2020.08.011.

Otten, R., Pádua, R. A. P., Bunzel, H. A., Nguyen, V., Pitsawong, W., Patterson, M., ... Kern, D. (2020). How directed evolution reshapes the energy landscape in an enzyme to boost catalysis. *Science (New York, N. Y.), 370*(6523), 1442–1446. https://doi.org/10.1126/science.abd3623.

Owen, R. L., Axford, D., Sherrell, D. A., Kuo, A., Ernst, O. P., Schulz, E. C., ... Mueller-Werkmeister, H. M. (2017). Low-dose fixed-target serial synchrotron crystallography. *Acta Crystallographica. Section D, Structural Biology, 73*(Pt 4), 373–378. https://doi.org/10.1107/S2059798317002996.

Palmer, K. F., & Williams, D. (1974). Optical properties of water in the near infrared. *JOSA, 64*(8), 1107–1110. https://doi.org/10.1364/JOSA.64.001107.

Park, S.-Y., Choi, H., Eo, C., Cho, Y., & Nam, K. H. (2020). Fixed-target serial synchrotron crystallography using Nylon mesh and enclosed film-based sample holder. *Crystals, 10*(9), 9. https://doi.org/10.3390/cryst10090803.

Perry, S. L., Guha, S., Pawate, A. S., Henning, R., Kosheleva, I., Srajer, V., ... Ren, Z. (2014). In situ serial Laue diffraction on a microfluidic crystallization device. *Journal of Applied Crystallography, 47*(Pt 6), 1975–1982. https://doi.org/10.1107/S1600576714023322.

Pflugrath, J. W. (2015). Practical macromolecular cryocrystallography. *Acta Crystallographica. Section F, Structural Biology Communications, 71*(Pt 6), 622–642. https://doi.org/10.1107/S2053230X15008304.

Phillips, R. S., Miles, E. W., McPhie, P., Marchal, S., Georges, C., Dupont, Y., & Lange, R. (2008). Pressure and temperature jump relaxation kinetics of the conformational change in Salmonella typhimurium Tryptophan synthase l-serine complex: Large activation compressibility and heat capacity changes demonstrate the contribution of solvation. *Journal of the American Chemical Society, 130*(41), 13580–13588. https://doi.org/10.1021/ja8018466.

Phillips, W. C., Li, Y., Stanton, M., Xie, J., O'Mara, D., & Kalata, K. (1993). A CCD-based area detector for X-ray crystallography using synchrotron and laboratory sources. *Nuclear Instruments and Methods in Physics Research Section A: Accelerators, Spectrometers, Detectors and Associated Equipment, 334*(2), 621–630. https://doi.org/10.1016/0168-9002(93)90830-B.

Polsinelli, I., Savko, M., Rouanet-Mehouas, C., Ciccone, L., Nencetti, S., Orlandini, E., ... Shepard, W. (2017). Comparison of helical scan and standard rotation methods in single-crystal X-ray data collection strategies. *Journal of Synchrotron Radiation, 24*(1), 1. https://doi.org/10.1107/S1600577516018488.

Rajashankar, K., & Dauter, Z. (2014). Data collection for crystallographic structure determination. *Methods in Molecular Biology (Clifton, N. J.), 1140*, 211–237. https://doi.org/10.1007/978-1-4939-0354-2_17.

Riley, B. T., Wankowicz, S. A., De Oliveira, S. H. P., Van Zundert, G. C. P., Hogan, D. W., Fraser, J. S., ... Van Den Bedem, H. (2021). qFit 3: Protein and ligand multi-conformer modeling for X-ray crystallographic and single-particle cryo-EM density maps. *Protein Science: A Publication of the Protein Society, 30*(1), 270–285. https://doi.org/10.1002/pro.4001.

Rimmerman, D., Leshchev, D., Hsu, D. J., Hong, J., Abraham, B., Kosheleva, I., ... Chen, L. X. (2018). Insulin hexamer dissociation dynamics revealed by photoinduced T-jumps and time-resolved X-ray solution scattering. *Photochemical & Photobiological Sciences, 17*(7), 874–882. https://doi.org/10.1039/c8pp00034d.

Rimmerman, D., Leshchev, D., Hsu, D. J., Hong, J., Kosheleva, I., & Chen, L. X. (2017). Direct observation of insulin association dynamics with time-resolved X-ray scattering. *The Journal of Physical Chemistry Letters, 8*(18), 4413–4418. https://doi.org/10.1021/acs.jpclett.7b01720.

Ringe, D., & Petsko, G. A. (1986). *[19]Study of protein dynamics by X-ray diffraction. Methods in Enzymology, 131*, Academic Press, 389–433. ⟨https://doi.org/10.1016/0076-6879(86)31050-4⟩.

Roedig, P., Duman, R., Sanchez-Weatherby, J., Vartiainen, I., Burkhardt, A., Warmer, M., ... Meents, A. (2016). Room-temperature macromolecular crystallography using a micro-patterned silicon chip with minimal background scattering. *Journal of Applied Crystallography, 49*(Pt 3), 968–975. https://doi.org/10.1107/S1600576716006348.

Roedig, P., Ginn, H. M., Pakendorf, T., Sutton, G., Harlos, K., Walter, T. S., ... Meents, A. (2017). High-speed fixed-target serial virus crystallography. *Nature Methods, 14*(8), 805–810. https://doi.org/10.1038/nmeth.4335.

Roedig, P., Vartiainen, I., Duman, R., Panneerselvam, S., Stübe, N., Lorbeer, O., ... Meents, A. (2015). A micro-patterned silicon chip as sample holder for macromolecular crystallography experiments with minimal background scattering. *Scientific Reports, 5*, 10451. https://doi.org/10.1038/srep10451.

Roessler, C. G., Agarwal, R., Allaire, M., Alonso-Mori, R., Andi, B., Bachega, J. F. R., ... Zouni, A. (2016). Acoustic injectors for drop-on-demand serial femtosecond crystallography. *Structure (London, England: 1993), 24*(4), 631–640. https://doi.org/10.1016/j.str.2016.02.007.

Rossmann, M. G., Leslie, A. G. W., Abdel-Meguid, S. S., & Tsukihara, T. (1979). Processing and post-refinement of oscillation camera data. *Journal of Applied Crystallography, 12*(6), 6. https://doi.org/10.1107/S0021889879013273.

Rubtsov, I. V., & Burin, A. L. (2019). Ballistic and diffusive vibrational energy transport in molecules. *The Journal of Chemical Physics, 150*(2), 020901. https://doi.org/10.1063/1.5055670.

Russi, S., González, A., Kenner, L. R., Keedy, D. A., Fraser, J. S., & van den Bedem, H. (2017). Conformational variation of proteins at room temperature is not dominated by radiation damage. *Journal of Synchrotron Radiation, 24*(Pt 1), 73–82. https://doi.org/10.1107/S1600577516017343.

Saha, S., Özden, C., Samkutty, A., Russi, S., Cohen, A., Stratton, M. M., & Perry, S. L. (2023). Polymer-based microfluidic device for on-chip counter-diffusive crystallization and in situ X-ray crystallography at room temperature. *Lab on a Chip, 23*(8), 2075–2090. https://doi.org/10.1039/d2lc01194h.

Sandalova, T., Schneider, G., Käck, H., & Lindqvist, Y. (1999). Structure of dethiobiotin synthetase at 0.97 A resolution. *Acta Crystallographica. Section D, Biological Crystallography, 55*(Pt 3), 610–624. https://doi.org/10.1107/s090744499801381x.

Scheidig, A. J., Burmester, C., & Goody, R. S. (1999). The pre-hydrolysis state of p21(ras) in complex with GTP: New insights into the role of water molecules in the GTP hydrolysis reaction of ras-like proteins. *Structure (London, England: 1993), 7*(11), 1311–1324. https://doi.org/10.1016/s0969-2126(00)80021-0.

Schlichting, I. (2015). Serial femtosecond crystallography: The first five years. *IUCrJ, 2*(Pt 2), 246–255. https://doi.org/10.1107/S205225251402702X.

Schmidt, M., Graber, T., Henning, R., & Srajer, V. (2010). Five-dimensional crystallography. *Acta Crystallographica. Section A, Foundations of Crystallography, 66*(2), 198–206. https://doi.org/10.1107/S0108767309054166.

Schulz, E. C., Yorke, B. A., Pearson, A. R., & Mehrabi, P. (2022). Best practices for time-resolved serial synchrotron crystallography. *Acta Crystallographica. Section D, Structural Biology, 78*(1), 14–29. https://doi.org/10.1107/S2059798321011621.

Shaikevitch, A., & Kam, Z. (1981). Investigation of long-range order in protein crystals by X-ray diffraction. *Acta Crystallographica. Section A, Crystal Physics, Diffraction, Theoretical and General Crystallography, 37*(6), 6. https://doi.org/10.1107/S0567739481001897.

Shimazu, Y., Tono, K., Tanaka, T., Yamanaka, Y., Nakane, T., Mori, C., ... Yabashi, M. (2019). High-viscosity sample-injection device for serial femtosecond crystallography at atmospheric pressure. *Journal of Applied Crystallography, 52*(6), 1280–1288. https://doi.org/10.1107/S1600576719012846.

Sierra, R. G., Gati, C., Laksmono, H., Dao, E. H., Gul, S., Fuller, F., ... DeMirci, H. (2016). Concentric-flow electrokinetic injector enables serial crystallography of ribosome and photosystem-II. *Nature Methods, 13*(1), 59–62. https://doi.org/10.1038/nmeth.3667.

Singh, B., Miller, S. R., Bhandari, H. B., Graceffa, R., Irving, T. C., & Nagarkar, V. V. (2013). High-speed detector for time-resolved diffraction studies. *Journal of Physics. Conference Series, 425*(9), 092005. https://doi.org/10.1088/1742-6596/425/9/092005.

Skaist Mehlman, T., Biel, J. T., Azeem, S. M., Nelson, E. R., Hossain, S., Dunnett, L., ... Keedy, D. A. (2023). Room-temperature crystallography reveals altered binding of small-molecule fragments to PTP1B. *ELife, 12*, e84632. https://doi.org/10.7554/eLife.84632.

Soares, A. S., Yamada, Y., Jakoncic, J., McSweeney, S., Sweet, R. M., Skinner, J., ... Bernstein, H. J. (2022). Serial crystallography with multi-stage merging of thousands of images. *Acta Crystallographica Section F: Structural Biology Communications, 78*(7), 7. https://doi.org/10.1107/S2053230X22006422.

Šrajer, V., & Schmidt, M. (2017). Watching proteins function with time-resolved X-ray crystallography. *Journal of Physics D: Applied Physics, 50*(37), 373001. https://doi.org/10.1088/1361-6463/aa7d32.

Steller, I., Bolotovsky, R., & Rossmann, M. G. (1997). An algorithm for automatic indexing of oscillation images using Fourier analysis. *Journal of Applied Crystallography, 30*(6), 6. https://doi.org/10.1107/S0021889897008777.

Stinton, G. W., & Evans, J. S. O. (2007). Parametric Rietveld refinement. *Journal of Applied Crystallography, 40*(Pt 1), 87–95. https://doi.org/10.1107/S0021889806043275.

Sugahara, M., Nakane, T., Masuda, T., Suzuki, M., Inoue, S., Song, C., ... Iwata, S. (2017). Hydroxyethyl cellulose matrix applied to serial crystallography. *Scientific Reports, 7*(1), 703. https://doi.org/10.1038/s41598-017-00761-0.

Sui, S., Mulichak, A., Kulathila, R., McGee, J., Filiatreault, D., Saha, S., ... Perry, S. L. (2021). A capillary-based microfluidic device enables primary high-throughput room-temperature crystallographic screening. *Journal of Applied Crystallography, 54*(4), 1034–1046. https://doi.org/10.1107/S1600576721004155.

Thompson, M. C., Barad, B. A., Wolff, A. M., Sun Cho, H., Schotte, F., Schwarz, D. M. C., ... Fraser, J. S. (2019). Temperature-jump solution X-ray scattering reveals distinct motions in a dynamic enzyme. *Nature Chemistry, 11*(11), 1058–1066. https://doi.org/10.1038/s41557-019-0329-3.

Thompson, M. C., Cascio, D., & Yeates, T. O. (2018). Microfocus diffraction from different regions of a protein crystal: Structural variations and unit-cell polymorphism. *Acta Crystallographica. Section D, Structural Biology, 74*(Pt 5), 411–421. https://doi.org/10.1107/S2059798318003479.

Thompson, M. C., Yeates, T. O., & Rodriguez, J. A. (2020). Advances in methods for atomic resolution macromolecular structure determination. *F1000Research*, *9*, F1000 Faculty Rev-667. ⟨https://doi.org/10.12688/f1000research.25097.1⟩.

Thorne, R. E. (2023). Determining biomolecular structures near room temperature using X-ray crystallography: Concepts, methods and future optimization. *Acta Crystallographica. Section D, Structural Biology, 79*(1), 1. https://doi.org/10.1107/S2059798322011652.

Tilton, R. F., Jr., Dewan, J. C., & Petsko, G. A. (1992). Effects of temperature on protein structure and dynamics: X-ray crystallographic studies of the protein ribonuclease-A at nine different temperatures from 98 to 320K. *Biochemistry, 31*(9), 2469–2481. https://doi.org/10.1021/bi00124a006.

Ueno, G., Shimada, A., Yamashita, E., Hasegawa, K., Kumasaka, T., Shinzawa-Itoh, K., ... Yamamoto, M. (2019). Low-dose X-ray structure analysis of cytochrome c oxidase utilizing high-energy X-rays. *Journal of Synchrotron Radiation, 26*(Pt 4), 912–921. https://doi.org/10.1107/S1600577519006805.

Uervirojnangkoorn, M., Zeldin, O. B., Lyubimov, A. Y., Hattne, J., Brewster, A. S., Sauter, N. K., ... Weis, W. I. (2015). Enabling X-ray free electron laser crystallography for challenging biological systems from a limited number of crystals. *ELife, 4*, e05421. https://doi.org/10.7554/eLife.05421.

Ursby, T., & Bourgeois, D. (1997). Improved estimation of structure-factor difference amplitudes from poorly accurate data. *Acta Crystallographica. Section A, Foundations of Crystallography, 53*(5), 5. https://doi.org/10.1107/S0108767397004522.

Vahedi-Faridi, A., Lovelace, J., Bellamy, H. D., Snell, E. H., & Borgstahl, G. E. O. (2003). Physical and structural studies on the cryocooling of insulin crystals. *Acta Crystallographica. Section D, Biological Crystallography, 59*(Pt 12), 2169–2182. https://doi.org/10.1107/s0907444903019668.

Vakili, M., Vasireddi, R., Gwozdz, P. V., Monteiro, D. C. F., Heymann, M., Blick, R. H., & Trebbin, M. (2020). Microfluidic polyimide gas dynamic virtual nozzles for serial crystallography. *Review of Scientific Instruments, 91*(8), 085108. https://doi.org/10.1063/5.0012806.

Van Den Bedem, H., Dhanik, A., Latombe, J. C., & Deacon, A. M. (2009). Modeling discrete heterogeneity in X-ray diffraction data by fitting multi-conformers. *Acta Crystallographica. Section D, Biological Crystallography, 65*(Pt 10), 1107–1117. https://doi.org/10.1107/S0907444909030613.

Wall, M. E., Wolff, A. M., & Fraser, J. S. (2018). Bringing diffuse X-ray scattering into focus. *Current Opinion in Structural Biology, 50*, 109–116. https://doi.org/10.1016/j.sbi.2018.01.009.

Warkentin, M., & Thorne, R. E. (2007). A general method for hyperquenching protein crystals. *Journal of Structural and Functional Genomics, 8*(4), 141–144. https://doi.org/10.1007/s10969-007-9029-0.

Warkentin, M., & Thorne, R. E. (2009). Slow cooling of protein crystals. *Journal of Applied Crystallography, 42*(Pt 5), 944–952. https://doi.org/10.1107/S0021889809023553.

Warren, A. J., Crawshaw, A. D., Trincao, J., Aller, P., Alcock, S., Nistea, I., ... Evans, G. (2015). In vacuo X-ray data collection from graphene-wrapped protein crystals. *Acta Crystallographica. Section D, Biological Crystallography, 71*(Pt 10), 2079–2088. https://doi.org/10.1107/S1399004715014194.

Weierstall, U., James, D., Wang, C., White, T. A., Wang, D., Liu, W., ... Cherezov, V. (2014). Lipidic cubic phase injector facilitates membrane protein serial femtosecond crystallography. *Nature Communications, 5*(1), 3309. https://doi.org/10.1038/ncomms4309.

Weik, M., & Colletier, J.-P. (2010). Temperature-dependent macromolecular X-ray crystallography. *Acta Crystallographica. Section D, Biological Crystallography, 66*(Pt 4), 437–446. https://doi.org/10.1107/S0907444910002702.

Weik, M., Kryger, G., Schreurs, A. M., Bouma, B., Silman, I., Sussman, J. L., ... Kroon, J. (2001). Solvent behaviour in flash-cooled protein crystals at cryogenic temperatures. *Acta Crystallographica. Section D, Biological Crystallography, 57*(Pt 4), 566–573. https://doi.org/10.1107/s0907444901001196.

Weinert, T., Olieric, N., Cheng, R., Brünle, S., James, D., Ozerov, D., ... Standfuss, J. (2017). Serial millisecond crystallography for routine room-temperature structure determination at synchrotrons. *Nature Communications, 8*(1), 1. https://doi.org/10.1038/s41467-017-00630-4.

White, T. A. (2014). Post-refinement method for snapshot serial crystallography. *Philosophical Transactions of the Royal Society B: Biological Sciences, 369*(1647), 20130330. https://doi.org/10.1098/rstb.2013.0330.

White, T. A. (2019). Processing serial crystallography data with CrystFEL: A step-by-step guide. *Acta Crystallographica. Section D, Structural Biology, 75*(2), 219–233. https://doi.org/10.1107/S205979831801238X.

Wickstrand, C., Katona, G., Nakane, T., Nogly, P., Standfuss, J., Nango, E., & Neutze, R. (2020). A tool for visualizing protein motions in time-resolved crystallography. *Structural Dynamics (Melville, N. Y.), 7*(2), 024701. https://doi.org/10.1063/1.5126921.

Wilson, M. A. (2022). Mapping enzyme landscapes by time-resolved crystallography with synchrotron and X-ray free electron laser light. *Annual Review of Biophysics, 51*(1), 79–98. https://doi.org/10.1146/annurev-biophys-100421-110959.

Winkler, F. K., Schutt, C. E., & Harrison, S. C. (1979). The oscillation method for crystals with very large unit cells. *Acta Crystallographica. Section A, Crystal Physics, Diffraction, Theoretical and General Crystallography, 35*(6), 6. https://doi.org/10.1107/S0567739479002035.

Winter, G., Gildea, R. J., Paterson, N. G., Beale, J., Gerstel, M., Axford, D., ... Hall, D. R. (2019). How best to use photons. *Acta Crystallographica. Section D, Structural Biology, 75*(Pt 3), 242–261. https://doi.org/10.1107/S2059798319003528.

Winter, G., Waterman, D. G., Parkhurst, J. M., Brewster, A. S., Gildea, R. J., Gerstel, M., ... Evans, G. (2018). DIALS: Implementation and evaluation of a new integration package. *Acta Crystallographica. Section D, Structural Biology, 74*(Pt 2), 85–97. https://doi.org/10.1107/S2059798317017235.

Wolff, A. M., Nango, E., Young, I. D., Brewster, A. S., Kubo, M., Nomura, T., … Thompson, M.C. (2022). Mapping protein dynamics at high-resolution with temperature-jump X-ray crystallography. *bioRxiv*. 2022.06.10.495662. ⟨https://doi.org/10.1101/2022.06.10.495662⟩.

Wolff, A. M., Young, I. D., Sierra, R. G., Brewster, A. S., Martynowycz, M. W., Nango, E., ... Thompson, M. C. (2020). Comparing serial X-ray crystallography and microcrystal electron diffraction (MicroED) as methods for routine structure determination from small macromolecular crystals. *IUCrJ, 7*(Pt 2), 306–323. https://doi.org/10.1107/S205225252000072X.

Wu, H., & Arnold, E. (2019). Michael G. Rossmann (1930-2019). *Nature Structural & Molecular Biology, 26*(8), 660–662. https://doi.org/10.1038/s41594-019-0271-5.

Yabukarski, F., Doukov, T., Mokhtari, D. A., Du, S., & Herschlag, D. (2021). Damaged goods? Evaluating the impact of X-ray damage on conformational heterogeneity in room temperature and cryo-cooled protein crystals. *bioRxiv*. 2021.06.27.450091. ⟨https://doi.org/10.1101/2021.06.27.450091⟩.

Zarrine-Afsar, A., Barends, T. R. M., Müller, C., Fuchs, M. R., Lomb, L., Schlichting, I., & Miller, R. J. D. (2012). Crystallography on a chip. *Acta Crystallographica. Section D, Biological Crystallography, 68*(Pt 3), 321–323. https://doi.org/10.1107/S0907444911055296.

Zeldin, O. B., Brewster, A. S., Hattne, J., Uervirojnangkoorn, M., Lyubimov, A. Y., Zhou, Q., ... Brunger, A. T. (2015). Data Exploration Toolkit for serial diffraction experiments. *Acta Crystallographica. Section D, Biological Crystallography, 71*(Pt 2), 352–356. https://doi.org/10.1107/S1399004714025875.

Zwart, P. H., Afonine, P. V., Grosse-Kunstleve, R. W., Hung, L.-W., Ioerger, T. R., McCoy, A. J., ... Adams, P. D. (2008). Automated structure solution with the PHENIX suite. *Methods in Molecular Biology (Clifton, N. J.), 426*, 419–435. https://doi.org/10.1007/978-1-60327-058-8_28.